Pontifícia Universidade Católica
do Rio de Janeiro

Lucas Lima Vaz Jannuzzi

Study of the Point Matching Method for Modeling Tunnels with Deformed Arbitrary Cross Section, and Truncated by Impedance Boundary Condition

Dissertação de Mestrado

Thesis presented to the Programa de Pós–graduação em Engenharia de Elétrica, do Departamento de Engenharia Elétrica da PUC-Rio in partial fulfillment of the requirements for the degree of Mestre em Engenharia de Elétrica.

Advisor : Prof. José Ricardo Bergmann
Co-advisor: Prof. Guilherme Simon da Rosa

Rio de Janeiro
February 2025

Pontifícia Universidade Católica
do Rio de Janeiro

Lucas Lima Vaz Jannuzzi

Study of the Point Matching Method for Modeling Tunnels with Deformed Arbitrary Cross Section, and Truncated by Impedance Boundary Condition

Thesis presented to the Programa de Pós–graduação em Engenharia de Elétrica da PUC-Rio in partial fulfillment of the requirements for the degree of Mestre em Engenharia de Elétrica. Approved by the Examination Committee:

Prof. José Ricardo Bergmann
Advisor
Departamento de Engenharia Elétrica – PUC-Rio

Prof. Guilherme Simon da Rosa
Dep. de Eng. Eletrônica e de Telecomunicações – UNESP

Prof. Rafael Abrantes Penchel
Dep. de Eng. Eletrônica e de Telecomunicações – UNESP

Prof. Raul Oliveira Ribeiro
Dep. de Eng. Eletrônica e de Telecomunicações – UNESP

Rio de Janeiro, February the 26th, 2025

Lucas Lima Vaz Jannuzzi

Received the B.S. degree in electrical engineering from the Pontifical Catholic University of Rio de Janeiro, Rio de Janeiro, Brazil, in 2023

Bibliographic data

Jannuzzi, Lucas Lima Vaz

Study of the Point Matching Method for Modeling Tunnels with Deformed Arbitrary Cross Section, and Truncated by Impedance Boundary Condition / Lucas Lima Vaz Jannuzzi; advisor: José Ricardo Bergmann; co-advisor: Guilherme Simon da Rosa. – 2025.

52 f: il. color. ; 30 cm

Dissertação (mestrado) - Pontifícia Universidade Católica do Rio de Janeiro, Departamento de Engenharia Elétrica, 2025.

Inclui bibliografia

1. Engenharia Elétrica – Teses. 2. Método de Point Matching. 3. Condição de contorno de impedância. 4. Alta impedância. 5. Campos eletromagnéticoss. I. Bergmann, José Ricardo. II. Rosa, Guilherme Simon da. III. Pontifícia Universidade Católica do Rio de Janeiro. Departamento de Engenharia Elétrica. IV. Título.

CDD: 620.11

To my parents, for all the support and affection.

Acknowledgments

Firstly, I would like to thank God for all the strength and opportunities I have had so far along my journey.

I would like to express my sincere gratitude to everyone in the PUC-Rio community who contributed to the development and completion of this master's thesis, especially my advisor José Ricardo Bergmann for all the support, help, and suggestions.

My immense gratitude to my co-advisor Guilherme Simon da Rosa for the motivation, guidance, and support throughout the research.

I also thank the members of the examination committee for their time and dedication in evaluating this work.

I am grateful to my family and friends for all the encouragement and support, especially to my parents Deise Lima Vaz Jannuzzi and Márcio Francisco Jannuzzi, and to my brother Pedro Lima Vaz Jannuzzi.

This study was financed in part by the Coordenação de Aperfeiçoamento de Pessoal de Nível Superior - Brasil (CAPES) - Finance Code 001.

This study was financed in part by the Fundação Carlos Chagas Filho de Amparo à Pesquisa do Estado do Rio de Janeiro, under the Mestrado Nota 10 program.

Abstract

Jannuzzi, Lucas Lima Vaz; Bergmann, José Ricardo (Advisor); Rosa, Guilherme Simon da (Co-Advisor). **Study of the Point Matching Method for Modeling Tunnels with Deformed Arbitrary Cross Section, and Truncated by Impedance Boundary Condition**. Rio de Janeiro, 2025. 52p. Dissertação de Mestrado – Departamento de Engenharia Elétrica, Pontifícia Universidade Católica do Rio de Janeiro.

This work presents a theoretical analysis of a hollow waveguide with an arbitrarily shaped cross section, with straight longitudinal axis, and truncated by impedance boundary condition. Additionally, mathematical models for the electromagnetic characterization of guided millimeter waves are developed to apply the point matching method to solve the boundary value problem. In this context, a first-order Leontovich boundary condition is initially studied to determine the electromagnetic fields in a tunnel. To enhance the accuracy of the approximate solution of the Leontovich boundary condition, the use of the first-order Rytov boundary condition is proposed, considering the system's geometry (contour curvature). An algorithm involving the point matching technique was implemented in Matlab platform for the electromagnetic analysis inside the waveguide considering a constant surface impedance. The results of field propagation for different modes and conductivities are presented, discussed, and compared with finite element reference solutions.

Keywords

Point Matching Method; Impedance boundary condition; High impedance; Electromagnetic fields.

Resumo

Jannuzzi, Lucas Lima Vaz; Bergmann, José Ricardo; Rosa, Guilherme Simon da. **Estudo do Método de Point Matching para Modelamento de Túneis com Seção Transversal Arbitrária Deformada e Truncada por Condição de Contorno de Impedância**. Rio de Janeiro, 2025. 52p. Dissertação de Mestrado – Departamento de Engenharia Elétrica, Pontifícia Universidade Católica do Rio de Janeiro.

Este trabalho apresenta uma análise teórica do guia de onda oco com seção transversal de geometria arbitrária, eixo longitudinal reto e truncado por uma condição de contorno de impedância. Adicionalmente, modelos matemáticos para a caracterização eletromagnética de ondas milimétricas guiadas são desenvolvidos para a aplicação do método de point matching na resolução do problema de valor de contorno. Nesse sentido, é abordado um estudo da condição de contorno de Leontovich de 1º ordem para determinação dos campos eletromagnéticos em um túnel. Com o objetivo de tornar a solução aproximada para a condição de contorno de Leontovich mais precisa, é proposto o emprego da condição de contorno de Rytov de 1° ordem, levando em consideração a geometria do sistema (curvatura do contorno). Um algoritmo envolvendo a técnica de point matching foi implementado na plataforma Matlab para a análise eletromagnética dentro do guia considerando impedância de superfície constante. Os resultados dessa propagação dos campos para diferentes modos e condutividades são apresentados, discutidos e comparados com soluções de referência via elementos finitos.

Palavras-chave

Método de Point Matching; Condição de contorno de impedância; Alta impedância; Campos eletromagnéticos.

Table of contents

List of figures

List of tables

1
Introduction

1.1
General Introduction

The millimeter-wave band, covering frequencies between 30 GHz and 300 GHz, is the subject of numerous studies due to being a very challenging and interesting topic in the field of 5G, 6G, and future technologies. The analysis of electromagnetic wave propagation in waveguides with arbitrary cross sections has been studied in the literature for various applications such as tunnels, drillings, and wells. This analysis, within this frequency range, inside a tunnel with a cross-sectional area with discontinuities, or in other words, deformed geometry, can be conducted through approximate analytical techniques described by the authors in [1] and [2], or alternatively, based on an approximate solution using the semi-analytical method of point matching, considering that the tunnel is modeled as a waveguide truncated by a realistic impedance boundary condition with a straight longitudinal axis [3].

The history of impedance boundary conditions (IBCs) is discussed, at least partially, by Pelosi and Ufimtsev. While it is unclear who first introduced them, it is evident that both Shchukin and Leontovich deserve credit for what we will refer to as the zeroth-order impedance boundary conditions (in the case of Rytov's analysis, which is equivalent to the first order Leontovich boundary condition) [4]. The investigation of the electromagnetic characterization of high-frequency waves within tunnels of complex shapes is relevant due to the various applications in wireless communications, such as intelligent transportation systems and underground sensor networks. A simplified model for wave propagation in tunnels with absorbing walls can be obtained using constant impedance boundary conditions, as in [5], considering the circular shape. This example provides a good alternative for tunnels with highly absorbing concrete or rock walls, as it takes into account the formulation of only one layer. However, it is not very accurate due to the approximations of the surface impedance model.

When the tunnel has two layers (a two-layer coaxial guide), the model becomes more accurate by determining a discrete set of guided modes supported

in circular waveguides with losses. The author in [6] compares results from the exact solution of the two-layer tunnel problem with the approximate solution of a single-layer tunnel, via truncation by a first-order Leontovich impedance boundary condition. In [7], the author investigates the radio propagation characteristics in tunnels modeled as a two-layer circular waveguide with walls composed of soil.

In [8], an approach for incorporating surface roughness into models based on the vector parabolic equation method is studied, and thus, this perspective is applied to realistic tunnel geometries with arbitrary cross-sections and curvature variations. In simple scattering problems, where plane waves are incident on geometries with classic cross-sections such as circles and ellipses, closed-form solutions are shown in [9] and [10]. In this context, the mode matching technique (MMT) is widely used in the literature since, in simple geometries, the wave functions are known and boundary conditions are applied globally imposing field continuity on junction surfaces between different regions. Thus, in [11], the author applied the MMT to coupling structures, analyzing the influence of non-homogeneous dielectric loading on radiating structures. Additionally, this technique was used in lossy guided structures.

Scattering from other complex shapes (electromagnetic analysis in waveguides with non-canonical cross-sections) requires the use of brute-force methods such as the method of moments (MoM) [12], and the finite element method (FEM) [13, 14]. These techniques are widely used due to their relatively simple computational implementation, becoming popular, especially with their inclusion in several commercial 3D electromagnetic analysis and simulation software. Additionally, semi-analytical methods like point matching (PMM) [3,15,16], based on a series expansion in terms of special functions, can be used to satisfy boundary conditions in cylinders with cross-sections close to circular or elliptical shapes, where boundary conditions are imposed at discrete points along the contour, allowing to obtain an approximate solution to the two-dimensional Helmholtz equation with reduced computational requirements compared with brute force counterparts.

The thesis aims to develop new rigorous mathematical models for the characterization of a straight tunnel with arbitrary shape, and truncated by a Z impedance boundary condition, that is, to develop a solution that depends only geometry and environment information (tunnel walls). The mathematical formulation of the PMM to solve waveguides with arbitrary contours takes into account the effect of surface impedance which is constant for the scenario using the Leontovich boundary condition.

1.2 Dissertation Organization

The rest of this thesis is organized as described below. Chapter 2 briefly shows the theory of cylindrical wave functions to be used in problems whose boundaries coincide with surfaces defined by cylindrical coordinates.

In Chapter 3, we address a theoretical analysis of the waveguide with an arbitrary cross section shape, with a straight longitudinal axis, and truncated by an impedance boundary condition. Furthermore, using the boundary condition equation on a surface with high conductivity (1st order boundary condition or Leontovich boundary condition), expressions for the modal fields inside the guide are developed. The solution to the problem can be improved by using the 2nd order Rytov boundary condition, which is more accurate than the approximation of the solution for a truncated one-layer tunnel using the 1st order impedance boundary condition. However, as an additional future study, a simpler approximate simplification will be suggested: the 1st order solution of Rytov's Generalized Analysis, which takes into account the effect of curvature, different from the Leontovich boundary condition.

In Chapter 4, the point matching method will be used to solve the associated boundary value problem, and a numerical algorithm will be implemented in Matlab according to the formulation for Leontovich's 1st order impedance boundary condition.

Chapter 5 deals with the numerical results obtained for different cross-sectional geometries and different conductivities. Case studies of engineering applications such as microwave propagation in tunnels with arbitrary cross sections operating at a frequency of 1 GHz will be evaluated. The results obtained from the Leontovich boundary condition will be analyzed and compared with the finite element method (method used in the CST software simulation) and the perturbation method.

Appendix A presents a theoretical review of the 1st order Rytov boundary condition. The difference from the Leontovich boundary condition is that the field and surface impedance equations depend on a higher-order term and consider the effect of curvature.

In Chapter 6, the topics covered in this thesis are summarized, the conclusions of this work and suggestions for future research work are described.

2
Theoretical Review of Cylindrical Wave Functions

Homogeneous cylindrical devices can support various field configurations, including TE, TM, and hybrid modes. Problems with boundaries that coincide with cylindrical coordinate surfaces are typically solved in cylindrical coordinates. First, we consider solutions to the scalar Helmholtz equation. Once these scalar wave functions are obtained, we can construct electromagnetic fields.

The scalar Helmholtz equation is written as

$$\nabla^2\psi + k^2\psi = 0. \tag{2-1}$$

Expressing the Laplacian in cylindrical coordinates, we have

$$\frac{1}{\rho}\frac{\partial}{\partial\rho}\left(\rho\frac{\partial\psi}{\partial\rho}\right) + \frac{1}{\rho^2}\frac{\partial^2\psi}{\partial\phi^2} + \frac{\partial^2\psi}{\partial z^2} + k^2\psi = 0. \tag{2-2}$$

It is assumed that the solution ψ is separable into a product of functions that are dependent on a single coordinate. Thus, based on the variable separation method, we seek to find solutions in the form

$$\psi = R(\rho)\Phi(\phi)Z(z). \tag{2-3}$$

Dividing the above by ψ and substituting (2-3) into (2-2), it is possible to write

$$\frac{1}{\rho R}\frac{d}{d\rho}\left(\rho\frac{dR}{d\rho}\right) + \frac{1}{\rho^2\Phi}\frac{d^2\Phi}{d\phi^2} + \frac{1}{Z}\frac{d^2Z}{dz^2} + k^2 = 0. \tag{2-4}$$

where the third term is independet of ρ and ϕ. Furthermore, the equation must be null for all values of ρ, ϕ and z, so this term must also be independent of z. Therefore, we can define a constant k_z as

$$\frac{1}{Z}\frac{d^2Z}{dz^2} = -k_z^2. \tag{2-5}$$

Making the above substitution in (2-4) and taking the produt with ρ^2, we obtain

$$\frac{\rho}{R}\frac{d}{d\rho}\left(\rho\frac{dR}{d\rho}\right) + \frac{1}{\Phi}\frac{d^2\Phi}{d\phi^2} + (k^2 - k_z^2)\rho^2 = 0. \tag{2-6}$$

Now we have the second term of (2-6) as a function that is independent of ρ and z. All other terms are independent from ϕ. Again, since the equation must be null for all values of ρ, ϕ and z, we can do

$$\frac{1}{\Phi}\frac{d^2\Phi}{d\phi^2} = -n^2, \tag{2-7}$$

where n is a constant. The preceding equation then becomes an equation that depends only on ρ, that is,

$$\frac{\rho}{R}\frac{d}{d\rho}\left(\rho\frac{dR}{d\rho}\right) - n^2 + (k^2 - k_z^2)\rho^2 = 0. \tag{2-8}$$

The wave equation is now separated. We can define k_ρ as

$$k_\rho^2 = k^2 - k_z^2. \tag{2-9}$$

and write the separated equations [Eqs. (2-5), (2-7), and (2-8)] as

$$\rho\frac{d}{d\rho}\left(\rho\frac{dR}{d\rho}\right) + [(k_\rho\rho)^2 - n^2]R = 0, \tag{2-10}$$

$$\frac{d^2\Phi}{d\phi^2} + n^2\Phi = 0, \tag{2-11}$$

$$\frac{d^2Z}{dz^2} + k_z^2 Z = 0. \tag{2-12}$$

Equation (2-10) is a Bessel differential equation of order n, with the general solution given by the linear combination of Bessel and Hankel functions of first kind, i.e., $J_n(k_\rho\rho)$ and $H_n(k_\rho\rho)$, respectively. Based on the problem analyzed, the solution can be obtained using one of these functions or a linear combination of them. In this work, considering all the characteristics of the problem, we chose to use a solution given by $J_n(k_\rho\rho)$, since the origin $\rho = 0$ is within the domain of interest.

Equations (2-11) and (2-12) present harmonic functions as a solution, where the general solution was selected according to the problem studied. We will consider the elementary wave function in the form

$$\psi_{k_\rho,n,k_z} = J_n(k_\rho\rho)e^{jn\phi}e^{-jk_z z}. \tag{2-13}$$

and the final solution to the Helmholtz equation is given by a linear combination of all elementary wave functions that serve as a solution to the problem.

We can add all possible values of n and k_ρ (or k_z) taking into account the constants associated with a particular solution $\{n, k_\rho\}$ — A_{n,k_ρ} —, that is:

$$\psi_{k_\rho,n,k_z} = \sum_n \sum_{k_\rho} A_{n,k_\rho} J_n(k_\rho \rho) e^{jn\phi} e^{-jk_z z}. \tag{2-14}$$

Given that the solution ψ is known, we can calculate the value of the field components according to [15]. Therefore, the TM^z fields are given by

$$\begin{aligned} E_\rho &= \frac{1}{\tilde{y}} \frac{\partial^2 \psi}{\partial \rho \partial z} & H_\rho &= \frac{1}{\rho} \frac{\partial \psi}{\partial \phi} \\ E_\phi &= \frac{1}{\tilde{y}\rho} \frac{\partial^2 \psi}{\partial \phi \partial z} & H_\phi &= -\frac{\partial \psi}{\partial \rho} \\ E_z &= \frac{1}{\tilde{y}} \left(\frac{\partial^2}{\partial z^2} + k^2 \right) \psi & H_z &= 0 \end{aligned} \tag{2-15}$$

and the TE^z fields are expressed as

$$\begin{aligned} E_\rho &= -\frac{1}{\rho} \frac{\partial \psi}{\partial \phi} & H_\rho &= \frac{1}{\tilde{z}} \frac{\partial^2 \psi}{\partial \rho \partial z} \\ E_\phi &= \frac{\partial \psi}{\partial \rho} & H_\phi &= \frac{1}{\tilde{z}\rho} \frac{\partial^2 \psi}{\partial \phi \partial z} \\ E_z &= 0 & H_z &= \frac{1}{\tilde{z}} \left(\frac{\partial^2}{\partial z^2} + k^2 \right) \psi \end{aligned} \tag{2-16}$$

3
Approximate Boundary Conditions in Electromagnetism: Theory and Formulation

One of the most common boundary condition is the impedance boundary condition, which relates the tangential components of the electric and magnetic fields through a surface. The surface impedance boundary condition was first used in electromagnetic scattering by numerous russian authors in the early 1940s and is generally attributed to Leontovich, commonly referred to as the Leontovich boundary condition or first-order boundary condition. In 1939, Rytov made the first systematic attempt to address surface impedance boundary conditions. His perspective on the perturbation method allowed the calculation of fields inside and outside conductors based on power series expansions and included the Leontovich condition as the first-order term in the expansion. The inclusion of higher-order terms enables the treatment of curved boundaries as well as variations in the field on the surface of the conductors. The method is not as well-known as others, mainly because Rytov's work was published in russian. The work developed by Leontovich and the surface impedance boundary condition named after him are much more well-known and have wide acceptance to this day [17, 18].

Firstly, before presenting the expressions related to the boundary conditions, it is worth providing a brief explanation of the Leontovich boundary condition and the Generalized Rytov Analysis. Although they are similar concepts, there are different aspects in the approach of wave propagation problems and the context used.

The Leontovich boundary condition, which describes the relationship between the electric and magnetic fields on a highly conductive surface, is a specific form of boundary condition used in the analysis of electromagnetic problems that consider interfaces between dielectric media and highly conductive surfaces. Moreover, this boundary condition is based on a first-order approach [18].

On the other hand, the Rytov boundary condition, which is part of the Generalized Rytov Analysis, is a broader approach that models the propagation of electromagnetic waves in random media. In summary, while the Leontovich boundary condition focuses on the properties of interfaces between dielectrics

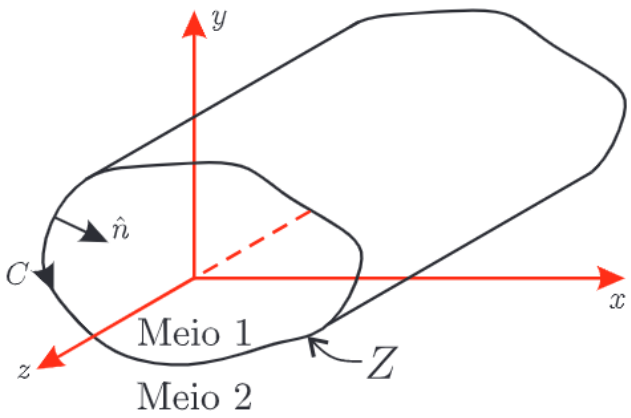

Figure 3.1: Hollow waveguide with arbitrary cross-section and truncated by impedance boundary condition Z.

and conductors, the Rytov boundary condition addresses wave propagation in random media, taking into account the statistical fluctuations of the medium, that is, it considers the contour curvature and impedance variation [19]. Therefore, the Rytov boundary condition deals with an anisotropic impedance, a boundary impedance that varies according to the direction of the field at the surface, that is, the value of the impedance depends on the orientation of the electric or magnetic field in relation to the preferred directions of the material or surface. This is especially important in waveguides with arbitrary cross-sections, where boundary conditions can vary in complex ways across the surface.

In this chapter, we will present the problem and framework used for developing the impedance boundary condition formulation on a high-order impedance surface.

3.1 First-Order Leontovich Boundary Condition

Consider the waveguide represented in Fig. 3.1 , where region 1 is the internal (uniform) part and region 2 is the external (conductive) part of the waveguide. The arbitrarily shaped contour C limits these regions. Defining the unit normal vector to the surface $\hat{n} = \hat{\rho}\, n_\rho + \hat{\phi}\, n_\phi$ pointing into the waveguide, and considering $Z = (\mu/\epsilon)^{1/2}$ as the impedance of the surrounding conductive medium (with $\mu = \mu_0$ and $\epsilon = \epsilon_0\epsilon_r - j\ \sigma/\omega$), we wish to impose the Leontovich impedance boundary condition [19]

$$\hat{n} \times \bar{E} = Z\ \hat{n} \times \left(\hat{n} \times \bar{H}\right) \tag{3-1}$$

on C.

Replacing the normal vector $\hat{n}$ in (3-1) and using the electromagnetic

fields with cylindrical components $\bar{E} = [E_\rho, E_\phi, E_z]^T$ e $\bar{H} = [H_\rho, H_\phi, H_z]^T$, we have that:

$$\left(\hat{\rho}\ n_\rho + \hat{\phi}\ n_\phi\right) \times \bar{E} = Z\ \left(\hat{\rho}\ n_\rho + \hat{\phi}\ n_\phi\right) \times \left(\left(\hat{\rho}\ n_\rho + \hat{\phi}\ n_\phi\right) \times \bar{H}\right) \quad (3\text{-}2)$$

$$\left(\hat{\rho}\ n_\rho + \hat{\phi}\ n_\phi\right) \times \left(\hat{\rho}\ E_\rho + \hat{\phi}\ E_\phi + \hat{z}\ E_z\right) = Z\ \left(\hat{\rho}\ n_\rho + \hat{\phi}\ n_\phi\right) \times \left(\left(\hat{\rho}\ n_\rho + \hat{\phi}\ n_\phi\right) \times \left(\hat{\rho}\ H_\rho + \hat{\phi}\ H_\phi + \hat{z}\ H_z\right)\right) \quad (3\text{-}3)$$

Solving the vector products in (3-3), we obtain the following:

$$\hat{z}\ n_\rho\ E_\phi - \hat{\phi}\ n_\rho\ E_z - \hat{z}\ n_\phi\ E_\rho + \hat{\rho}\ n_\phi\ E_z = Z\ \left(\hat{\rho}\ n_\rho + \hat{\phi}\ n_\phi\right) \times \left(\hat{z}\ n_\rho\ H_\phi - \hat{\phi}\ n_\rho\ H_z - \hat{z}\ n_\phi\ H_\rho + \hat{\rho}\ n_\phi\ H_z\right) \quad (3\text{-}4)$$

$$\hat{z}\,(n_\rho\ E_\phi - n_\phi\ E_\rho) - \hat{\phi}\ n_\rho\ E_z + \hat{\rho}\ n_\phi\ E_z = Z\ \left(\hat{\rho}\ n_\rho + \hat{\phi}\ n_\phi\right) \times \left[\hat{z}\,(n_\rho\ H_\phi - n_\phi\ H_\rho) - \hat{\phi}\ n_\rho\ H_z + \hat{\rho}\ n_\phi\ H_z\right] \quad (3\text{-}5)$$

$$\hat{z}\,(n_\rho\ E_\phi - n_\phi\ E_\rho) - \hat{\phi}\ n_\rho\ E_z + \hat{\rho}\ n_\phi\ E_z = Z\ \left[-\hat{\phi}\ n_\rho\,(n_\rho\ H_\phi - n_\phi\ H_\rho) - \hat{z}\ n_\rho^2\ H_z\right] + Z\left[\hat{\rho}\ n_\phi\,(n_\rho\ H_\phi - n_\phi\ H_\rho) - \hat{z}\ n_\phi^2\ H_z\right] \quad (3\text{-}6)$$

$$\hat{z}\,(n_\rho\ E_\phi - n_\phi\ E_\rho) - \hat{\phi}\ n_\rho\ E_z + \hat{\rho}\ n_\phi\ E_z = Z\ \left[\hat{\rho}\ n_\phi\,(n_\rho\ H_\phi - n_\phi\ H_\rho) - \hat{\phi}\ n_\rho\,(n_\rho\ H_\phi - n_\phi\ H_\rho)\right] - Z\ \left[\hat{z}\ \underbrace{\left(n_\rho^2 + n_\phi^2\right)}_{=1}\ H_z\right]. \quad (3\text{-}7)$$

Separating the components, in terms of $\hat{\rho}$, $\hat{\phi}$ and $\hat{z}$, we obtain, respectively

$$E_z = Z\ \left(n_\rho\ H_\phi - n_\phi\ H_\rho\right), \quad (3\text{-}8)$$

$$E_z = Z\ \left(n_\rho\ H_\phi - n_\phi\ H_\rho\right), \quad (3\text{-}9)$$

$$Z\ H_z = -n_\rho\ E_\phi + n_\phi\ E_\rho. \tag{3-10}$$

Note that the equations (3-8) and (3-9) are identical, and therefore we have only two linearly independent equations.

4
Point Matching Method (PMM)

The point-matching method is an effective approximate approach for solving problems in uniform waveguides and has been successfully applied in the analysis of various unconventional waveguide types. In this method, electromagnetic fields are evaluated at discrete points along the boundary surface. Boundary conditions are directly enforced at these points, resulting in a system of algebraic equations that relate the unknown field coefficients. It is a more straightforward and, in many cases, computationally simpler approach. The main advantage of PMM is that it does not require time-consuming and memory-intensive auxiliary calculations, which are typically necessary in other techniques such as MMT [22].

Although the point-matching method offers an efficient approach for solving boundary-value problems in waveguides with arbitrary cross-sectional geometries, it has certain limitations. One such restriction is that the cross section contour of the waveguide must be closed, as the wave function solutions represent closed contours that provide good approximations for the waveguide geometry. Furthermore, the function that describes the closed curve must be univocal in the radial direction ρ, meaning that for each fixed ϕ, there must be a single value of ρ on the same contour [23].

In this chapter, to study wave propagation in an air-filled waveguide, the point matching method is formulated according to the cylindrical wave functions described in the Chapter 2 and approached considering the Leontovich boundary condition.

4.1
PMM Using 1st Order Leontovich Boundary Condition

Using the point matching method, we can obtain a solution for Maxwell's equations with complex boundary conditions, by expanding the solutions of the electromagnetic field as a series of cylindrical harmonics [3]. However, if the waveguide surface does not coincide with the cylindrical coordinate surface, it is not possible to satisfy the boundary conditions *exactly*, and the expansions must be limited by a finite number of terms. Therefore, the boundary conditions are imposed at a finite set of points along the boundary

C between the domains of regions 1 and 2 as shown in Fig. 3.1.

Assuming and omitting the harmonic-temporal factor $\exp(+j\omega t)$, in cylindrical coordinates, the longitudinal fields can be written as [15]

$$E_z(\rho,\phi) = \sum_{-N}^{N} a_{en} J_n(k_\rho \rho) e^{jn\phi} \tag{4-1}$$

$$= \sum_{-N}^{N} e_z(\rho,\phi) a_{en} = \bar{e}_z^T(\rho,\phi)\,\bar{a}_{en}, \tag{4-2}$$

$$H_z(\rho,\phi) = \sum_{-N}^{N} a_{hn} J_n(k_\rho \rho) e^{jn\phi} \tag{4-3}$$

$$= \sum_{-N}^{N} h_z(\rho,\phi) a_{hn} = \bar{h}_z^T(\rho,\phi)\,\bar{a}_{hn}, \tag{4-4}$$

where J_n is the first kind Bessel function with integer order n. The expansions for E_z and H_z each have $2N+1$ harmonics, and therefore we have $2(2N+1)$ unknowns to solve. To solve them, we must consider at least one set with $2P = 2(2N+1)$ points along the perimeter of the waveguide. It is important to note that the propagation factor $e^{-jk_z z}$ was omitted when using only e_z and h_z as a function of ρ and ϕ.

Something similar to what was done above can be done to write the other field components — E_ρ, E_ϕ, H_ρ, and H_ϕ —, so that everything can be written in terms of the amplitude vectors a_{en} and a_{hn}. Defining

$$\bar{a} = \begin{bmatrix} \bar{a}_e \\ \bar{a}_h \end{bmatrix}, \tag{4-5}$$

we can establish the compact notation

$$E_\alpha = \begin{bmatrix} \bar{e}_{\alpha e}^T(\rho,\phi) & \bar{e}_{\alpha h}^T(\rho,\phi) \end{bmatrix} \bar{a},\ \alpha = \{\rho,\phi\}. \tag{4-6}$$

Based on (3-9), (3-10), (4-2), and (4-4), we can convert the boundary conditions to matrix form, such that

$$\begin{bmatrix} E_z \\ ZH_z \end{bmatrix} = \begin{bmatrix} \bar{e}_z^T & \bar{0}^T \\ \bar{0}^T & Z\bar{h}_z^T \end{bmatrix} \bar{a} = \begin{bmatrix} Z\bar{\Delta}_{\mathrm{TM},H_s}^T & Z\bar{\Delta}_{\mathrm{TE},H_s}^T \\ \bar{\Delta}_{\mathrm{TM},E_s}^T & \bar{\Delta}_{\mathrm{TE},E_s}^T \end{bmatrix} \bar{a}. \tag{4-7}$$

Above, the first matrix will be denoted as $\bar{\bar{M}}_{z1}$, and the second as $\bar{\bar{M}}_{z2}$. The Delta vectors will be defined in sequence, in (4-16)-(4-19). Thus, we can rewrite (4-7) as

$$\left[\bar{\bar{M}}_{z1}(\rho,\phi) - \bar{\bar{M}}_{z2}(\rho,\phi)\right] \bar{a} = \bar{0}. \tag{4-8}$$

Introducing $\bar{\bar{M}}(\rho,\phi) = \bar{\bar{M}}_{z1}(\rho,\phi) - \bar{\bar{M}}_{z2}(\rho,\phi)$, the boundary conditions on C can be written as

$$\bar{\bar{M}}(\rho,\phi)\bar{a} = \bar{0}. \tag{4-9}$$

In view of the point matching method, at a point p, at position (ρ_p,ϕ_p) on the contour C, we must impose

$$\bar{\bar{M}}(\rho_p,\phi_p)\bar{a} = \bar{0} \Rightarrow \bar{\bar{M}}_p\ \bar{a} = \bar{0}. \tag{4-10}$$

For $p = 1, 2, 3, \ldots, P$, we can impose the boundary conditions on all points by stacking all associated matrices $\bar{\bar{M}}_p$ into one generalized matrix $\bar{\bar{\bar{M}}}$, and establishing the nonlinear system of equations

$$\bar{\bar{\bar{M}}}\bar{a} = \bar{0}. \tag{4-11}$$

The eigenvalues k_ρ that solve the above problem are obtained by tracking the zeros of the characteristic equation $\det(\bar{\bar{\bar{M}}}) = 0$. For each eigenvalue found, the resolution of the null space of $\bar{\bar{\bar{M}}}$ will give an eigenvector $\bar{a}$, which allows recovering the modal amplitudes a_{en} and a_{hn} of the longitudinal fields in (4-1) and (4-3).

To fill in $\bar{\bar{M}}_{z2}$, we first multiply equation (2-15) by $\tilde{y}\,k_\rho^{-2}$, and equation (2-16) by $\tilde{z}\,k_\rho^{-2}$. With this normalization, we have the wave potentials $\psi^{\mathrm{TM}} = \bar{e}_z^T\bar{a}_e$ for the TM^z mode , and $\psi^{\mathrm{TE}} = \bar{h}_z^T\bar{a}_h$ for the TE^z mode. The impeditivity and admittivity were denoted here as $\tilde{z} = j\omega\mu$ and $\tilde{y} = j\omega\epsilon$, respectively, where μ is the magnetic permeability and ϵ is the electric permittivity. Thus, we can write the field components transversal to $\hat{z}$ as TM^z and TE^z contributions, as shown below.

$$E_\rho = \underbrace{\left(\frac{1}{k_\rho^2}\right)\left(\frac{\partial^2}{\partial\rho\,\partial z}\right)\bar{e}_z^T\bar{a}_e}_{\mathrm{TM}^z} + \underbrace{\left(\frac{\tilde{z}}{k_\rho^2}\right)\left(-\frac{1}{\rho}\frac{\partial}{\partial\phi}\right)\bar{h}_z^T\bar{a}_h}_{\mathrm{TE}^z} \tag{4-12}$$

$$E_\phi = \underbrace{\left(\frac{1}{k_\rho^2}\right)\left(\frac{1}{\rho}\frac{\partial^2}{\partial\phi\,\partial z}\right)\bar{e}_z^T\bar{a}_e}_{\mathrm{TM}^z} + \underbrace{\left(\frac{\tilde{z}}{k_\rho^2}\right)\left(\frac{\partial}{\partial\rho}\right)\bar{h}_z^T\bar{a}_h}_{\mathrm{TE}^z} \tag{4-13}$$

$$H_\rho = \underbrace{\left(\frac{\tilde{y}}{k_\rho^2}\right)\left(\frac{1}{\rho}\frac{\partial}{\partial\phi}\right)\bar{e}_z^T\bar{a}_e}_{\mathrm{TM}^z} + \underbrace{\left(\frac{1}{k_\rho^2}\right)\left(\frac{\partial^2}{\partial\rho\,\partial z}\right)\bar{h}_z^T\bar{a}_h}_{\mathrm{TE}^z} \tag{4-14}$$

$$H_\phi = \underbrace{\left(\frac{\tilde{y}}{k_\rho^2}\right)\left(-\frac{\partial}{\partial\rho}\right)\bar{e}_z^T\bar{a}_e}_{\mathrm{TM}^z} + \underbrace{\left(\frac{1}{k_\rho^2}\right)\left(\frac{1}{\rho}\frac{\partial^2}{\partial\phi\,\partial z}\right)\bar{h}_z^T\bar{a}_h}_{\mathrm{TE}^z} \tag{4-15}$$

Taking into account the fields defined in (4-12)-(4-15) and the boundary

conditions in (3-9) and (3-10), we have that the components of the matrix $\bar{\bar{M}}_{z2}$ can be written as follows:

$$\bar{\Delta}^T_{\mathrm{TM},H_s} = \left[n_\rho \underbrace{\left(\frac{\tilde{y}}{k_\rho^2}\right)\left(-\frac{\partial \bar{e}_z^T}{\partial \rho}\right)}_{H_\phi} - n_\phi \underbrace{\left(\frac{\tilde{y}}{k_\rho^2}\right)\left(\frac{1}{\rho}\frac{\partial \bar{e}_z^T}{\partial \phi}\right)}_{H_\rho} \right] \tag{4-16}$$

$$\bar{\Delta}^T_{\mathrm{TE},H_s} = \left[n_\rho \underbrace{\left(\frac{1}{k_\rho^2}\right)\left(\frac{1}{\rho}\frac{\partial^2 \bar{h}_z^T}{\partial \phi\ \partial z}\right)}_{H_\phi} - n_\phi \underbrace{\left(\frac{1}{k_\rho^2}\right)\left(\frac{\partial^2 \bar{h}_z^T}{\partial \rho\ \partial z}\right)}_{H_\rho} \right] \tag{4-17}$$

$$\bar{\Delta}^T_{\mathrm{TM},E_s} = \left[- n_\rho \underbrace{\left(\frac{1}{k_\rho^2}\right)\left(\frac{1}{\rho}\frac{\partial^2 \bar{e}_z^T}{\partial \phi\ \partial z}\right)}_{E_\phi} + n_\phi \underbrace{\left(\frac{1}{k_\rho^2}\right)\left(\frac{\partial^2 \bar{e}_z^T}{\partial \rho\ \partial z}\right)}_{E_\rho} \right] \tag{4-18}$$

$$\bar{\Delta}^T_{\mathrm{TE},E_s} = \left[- n_\rho \underbrace{\left(\frac{\tilde{z}}{k_\rho^2}\right)\left(\frac{\partial \bar{h}_z^T}{\partial \rho}\right)}_{E_\phi} + n_\phi \underbrace{\left(\frac{\tilde{z}}{k_\rho^2}\right)\left(-\frac{1}{\rho}\frac{\partial \bar{h}_z^T}{\partial \phi}\right)}_{E_\rho} \right] \tag{4-19}$$

The derivatives in terms of ρ, ϕ, and z above can be easily solved using $\partial[J_n(k_\rho\rho)]/\partial\rho \to k_\rho J_n'(k_\rho\rho)$, $\partial/\partial\phi \to jn$, and $\partial/\partial z \to -jk_z$. Thus, we have

$$\bar{\Delta}_{TM,H_s}|_n = - n_\rho \left(\frac{\tilde{y}}{k_\rho^2}\right)\left(k_\rho\ J_n'(k_\rho\rho)\ e^{jn\phi}\right) - n_\phi \left(\frac{\tilde{y}}{k_\rho^2}\right)\left(\frac{1}{\rho}\right)\left(j\ n\ J_n(k_\rho\rho)\ e^{jn\phi}\right), \tag{4-20}$$

$$\bar{\Delta}_{TE,H_s}|_n = n_\rho \left(\frac{1}{k_\rho^2}\right)\left(\frac{1}{\rho}\right)\left(n\ k_z\ J_n(k_\rho\rho)\ e^{jn\phi}\right) - n_\phi \left(\frac{1}{k_\rho^2}\right)\left(-j\ k_z\ k_\rho\ J_n'(k_\rho\rho)\ e^{jn\phi}\right), \tag{4-21}$$

$$\bar{\Delta}_{TM,E_s}|_n = - n_\rho \left(\frac{1}{k_\rho^2}\right)\left(\frac{1}{\rho}\right)\left(n\ k_z\ J_n(k_\rho\rho)\ e^{jn\phi}\right) + n_\phi \left(\frac{1}{k_\rho^2}\right)\left(-j\ k_z\ k_\rho\ J_n'(k_\rho\rho)\ e^{jn\phi}\right), \tag{4-22}$$

$$\bar{\Delta}_{TE,E_s}|_n = -\ n_\rho \left(\frac{\tilde{z}}{k_\rho^2}\right) \left(k_\rho\ J_n'(k_\rho\rho)\ e^{jn\phi}\right)\ - \\ n_\phi \left(\frac{\tilde{z}}{k_\rho^2}\right) \left(\frac{1}{\rho}\right) \left(j\ n\ J_n(k_\rho\rho)\ e^{jn\phi}\right). \quad (4\text{-}23)$$

5
Numerical Results

The mathematical formulation presented in previous chapters was implemented in an algorithm on the Matlab platform [24] in order to validate it and analyze the results obtained.

5.1
Results Using the Leontovich Boundary Condition

The results relating to the formulation based on Leontovich's 1st order boundary condition are shown below. Convergence was observed using $N = 8$ in all the scenarios investigated here.

5.1.1
Truncated Circular Waveguide with Imperfect Walls

We consider a circular waveguide with radius $a = 1$ m and $N = 8$ harmonics (with points equally spaced along the perimeter of the waveguide) in order to observe the electromagnetic propagation and identify the corresponding mode. The frequency used was 1 GHz.

5.1.1.1
Circular Waveguide with $\sigma_2 = 10^7$ S/m for the 1st Propagating Mode (Fundamental Mode)

In this scenario, a circular waveguide model with a mode index equal to 1 was used. When running the program for this example, the results were $E_{z_{\max}} = 0.1401$ and $H_{z_{\max}} = 0.80945$. Since there is a small portion of the electric field E_z associated with the amplitudes a_{en}, the mode becomes hybrid (a feature that can be captured in the perturbation approximations of [15]), meaning it is not a pure TE^z mode. Therefore, this is almost the TE^z_{11} mode ($E_{z_{\max}} < \eta\ H_{z_{\max}}$ with $\eta = 120\pi$), as evidenced by the longitudinal magnetic field shown in Fig. 5.1.

Another way to prove this mode is through the value of k_ρ found, considering that $k_\rho = x'_{np}/a$ and the radius a of the circular guide was fixed as 1 m. The value of k_ρ was $1.8409 + j\ 2.5604 \times 10^{-4}$ m^{-1}, practically equal to the value of $x'_{np} = x'_{11}$ in Table 5-3 of [15].

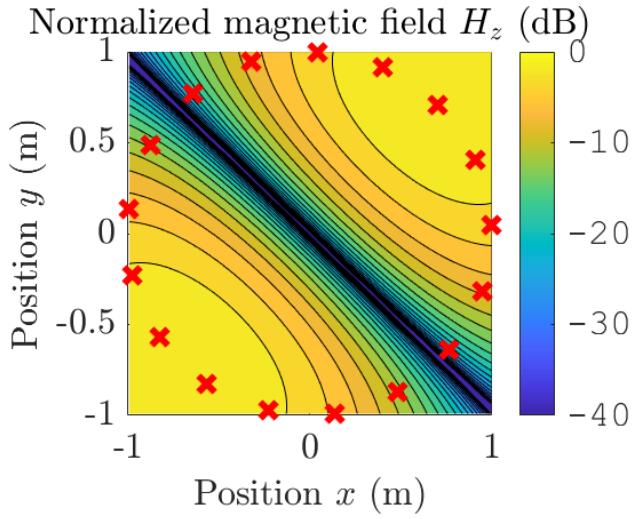

Figure 5.1: Normalized magnetic field H_z of mode 1 with $\sigma = 10^7$ S/m.

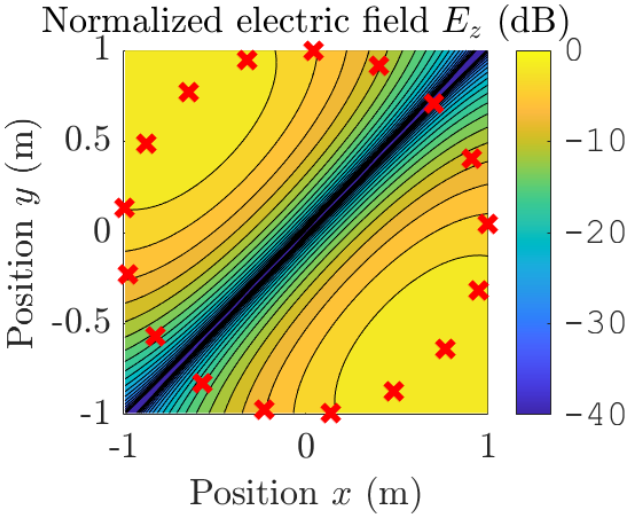

Figure 5.2: Normalized electric field E_z of mode 1 with $\sigma = 10^7$ S/m.

In Fig. 5.2 it is possible to observe the E_z field, orthogonal to the H_z field, as expected. There is another complementary field that shares the eigenvalue with this field, but is rotated by 90° with respect to that shown in Fig. 5.1.

Furthermore, to confirm the above, it is possible to analyze the electrical and magnetic modal amplitudes in Fig. 5.3. From them, it is observed that $a_e < \eta\ a_h$, once again confirming that this is almost the TE^z_{11} mode.

To validate our solution via the point matching method, we evaluated the effect of truncation of a good metal in region 2 by varying the electrical conductivity $\sigma_2 = \{10^3,\ 10^4,\ 10^5,\ 10^6,\ 10^7\}$ S/m. For reference, we compared our response to the solution via the contour-deformation perturbation method in [15], where the propagation constant for modes TM^z and TE^z is approxi-

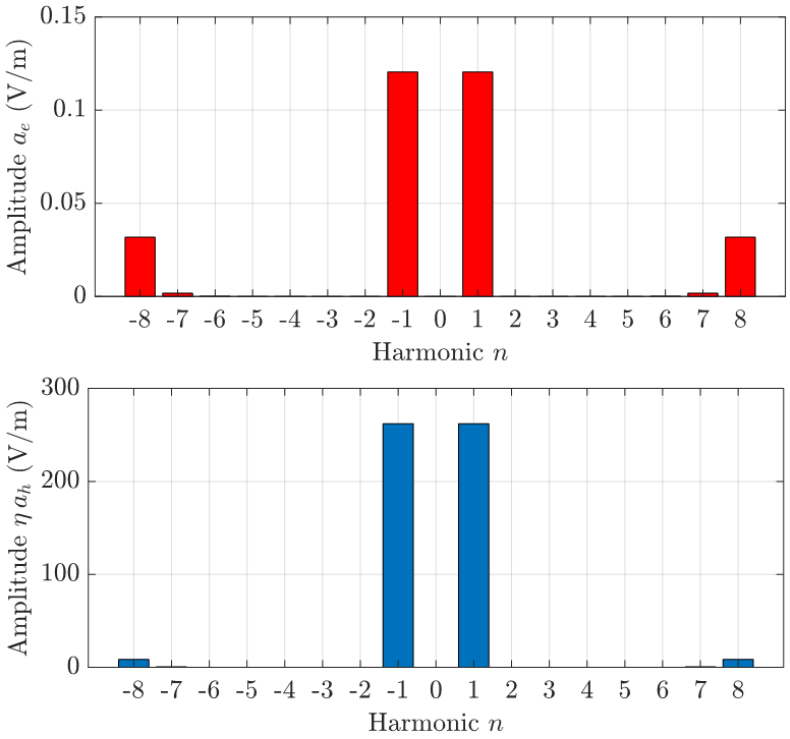

Figure 5.3: Modal amplitudes of mode 1 for the case $\sigma_2 = 10^7$ S/m.

mated by

$$jk_z \approx \alpha_c + j(\beta + \beta_c). \tag{5-1}$$

For TM^z modes, we have

$$\alpha_c = \frac{\Re e(Z)}{\eta\ a\ \sqrt{1-(f_c/f)^2}}, \tag{5-2}$$

$$\beta = [k^2 - (x_{np}/a)^2]^{1/2}, \tag{5-3}$$

$$\beta_c \approx \alpha_c. \tag{5-4}$$

For the TE^z modes, we have

$$\alpha_c = \frac{\Re e(Z)}{\eta\ a\ \sqrt{1-(f_c/f)^2}} \left[\frac{n^2}{(x'_{np})^2 - n^2} + \left(\frac{f_c}{f}\right)^2\right], \tag{5-5}$$

$$\beta = [k^2 - (x'_{np}/a)^2]^{1/2}, \tag{5-6}$$

$$\beta_c \approx \alpha_c. \tag{5-7}$$

Above, x_{np} and x'_{np} represent the p-th zeros of the Bessel function of order n and its derivative, respectively. Fig. 5.4 shows the longitudinal wavenumber of the first mode computed via the point matching solution and via the perturbation solution.

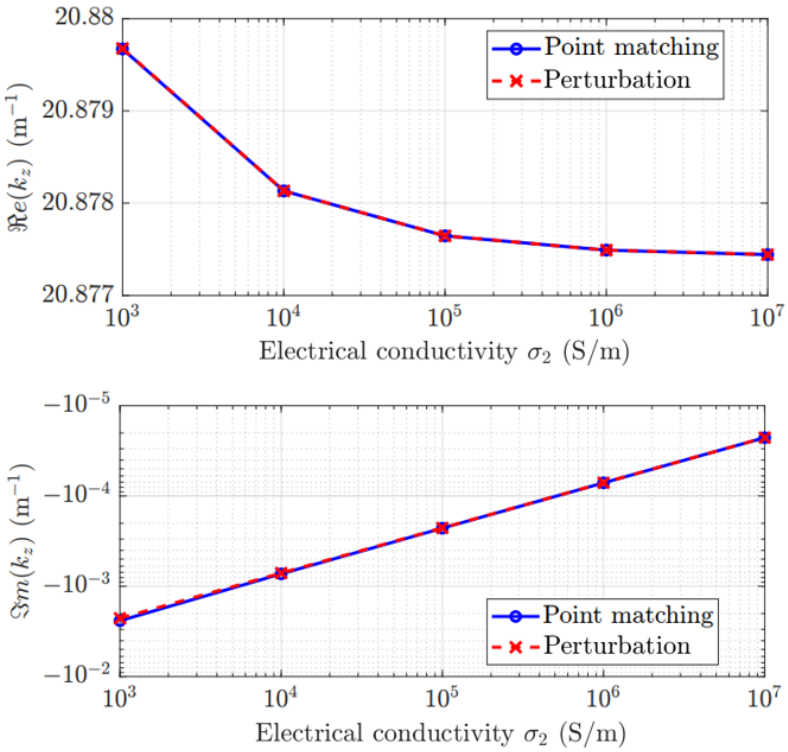

Figure 5.4: Longitudinal wavenumber of mode 1.

It is worth highlighting that unlike the perturbation solution, the modes computed by the technique explored here do not represent pure TM^z and TE^z fields. This is evidenced by the fundamental mode fields, whose modal amplitudes were shown in Fig. 5.3.

Finally, we compare our result with the reference solution obtained by the finite element method (FEM) of the CST software [25]. Fig. 5.5 shows the fields E_z and H_z via finite element solution in the CST. The presence of the axial electric field is associated with numerical errors in the FEM.

It is observed that the value of the longitudinal wave number k_z ($20.8774 - j\ 2.25783{\times}10^{-5}$ m^{-1}) was equal to that found by the point matching algorithm ($k_z = 20.877\ - j\ 2.2577 \times 10^{-5}$ m^{-1}).

5.1.1.2 Circular Waveguide with $\sigma_2 = 10^7$ S/m for the 2nd Propagating Mode

For the second mode, the maximum field amplitudes found in the algorithm were: $E_{z_{\max}} = 0.99995$ and $H_{z_{\max}} = 4.277 \times 10^{-8}$. Since there is a small contribution from the magnetic field, this is not the pure TM^z mode. Therefore, this is almost the TM^z_{01} mode ($E_{z_{\max}} > \eta\ H_{z_{\max}}$ with $\eta = 120\pi$), as observed in the longitudinal electric field in Fig. 5.6.

Another way to prove this mode is through the value of k_ρ found, considering that $k_\rho = x_{np}/a$ and the radius a of the circular guide was fixed

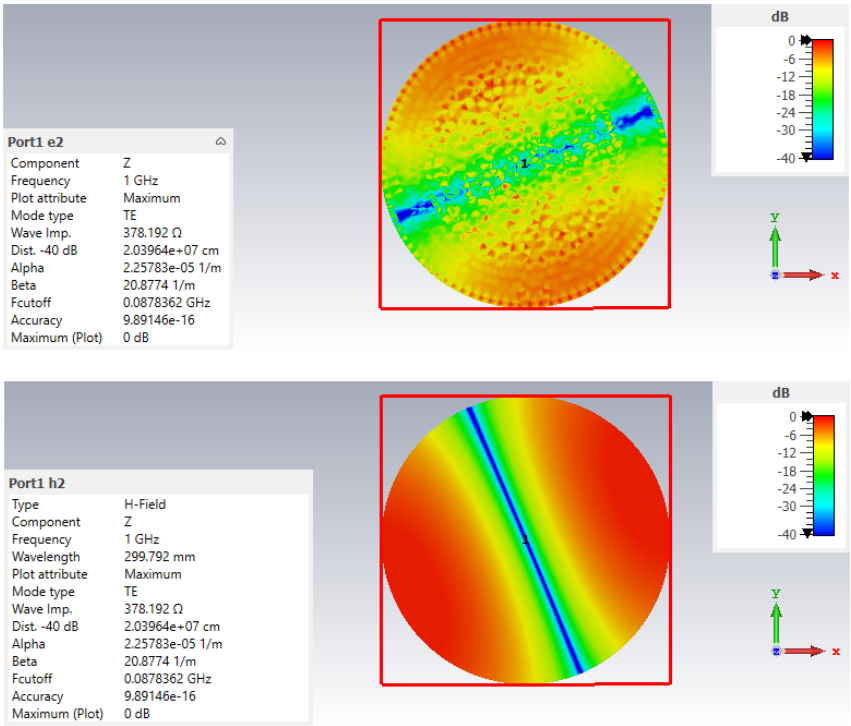

Figure 5.5: Normalized electric and magnetic fields E_z and H_z of mode 1 with $\sigma_2 = 10^7$ S/m via FEM.

as 1 m. The value of k_ρ was $2.4044 + j\ 4.5991 \times 10^{-4}$ m^{-1}, practically equal to the value of $x_{np} = x_{01}$ in Table 5-2 of [15].

Furthermore, from Fig. 5.7, it is noted that $a_e > \eta\ a_h$, therefore, this mode is almost the TM^z_{01} mode.

Fig. 5.8 shows the longitudinal wavenumber of the second mode computed via the point matching solution and via the perturbation solution.

Fig. 5.9 shows the fields E_z and H_z produced via the finite element solution in the CST for mode 2. Note that the value of the longitudinal wave number k_z is in agreement with that found by the point matching algorithm ($k_z = 20.820 - j\ 5.3112 \times 10^{-5}$ m^{-1}).

5.1.1.3 Circular Waveguide with $\sigma_2 = 10^7$ S/m for the 3rd Propagating Mode

For mode 3, when running the program, the results were $E_{z_{\max}} = 0.085275$ and $H_{z_{\max}} = 0.68234$. Since there is a portion of the maximum electric field, this is not the pure TE^z mode. Therefore, this is almost the TE^z_{21} mode ($E_{z_{\max}} < \eta\ H_{z_{\max}}$ with $\eta = 120\pi$), as evidenced in the longitudinal magnetic field in Fig. 5.10.

Another way to confirm this mode is through the value of k_ρ found, taking into account that $k_\rho = x'_{np}/a$ and the radius a of the circular guide was fixed

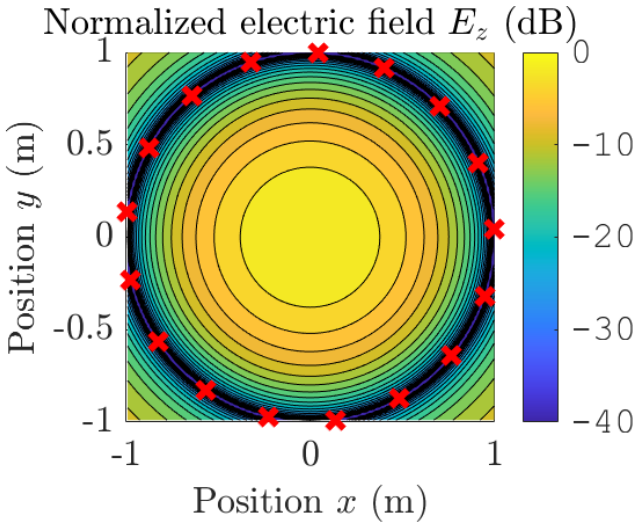

Figure 5.6: Normalized electric field E_z of mode 2 with $\sigma_2 = 10^7$ S/m.

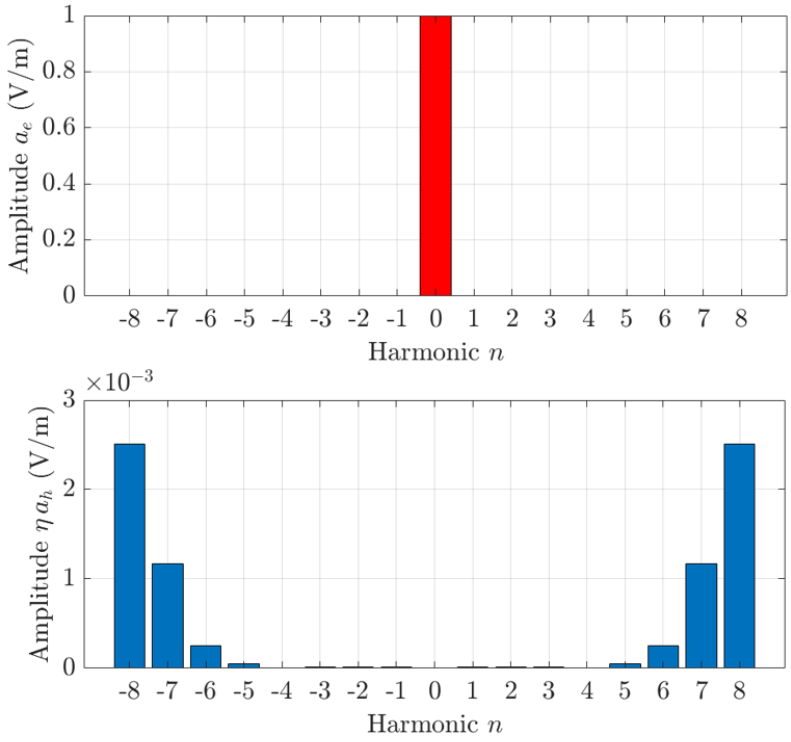

Figure 5.7: Modal amplitudes of mode 2 for the case $\sigma_2 = 10^7$ S/m.

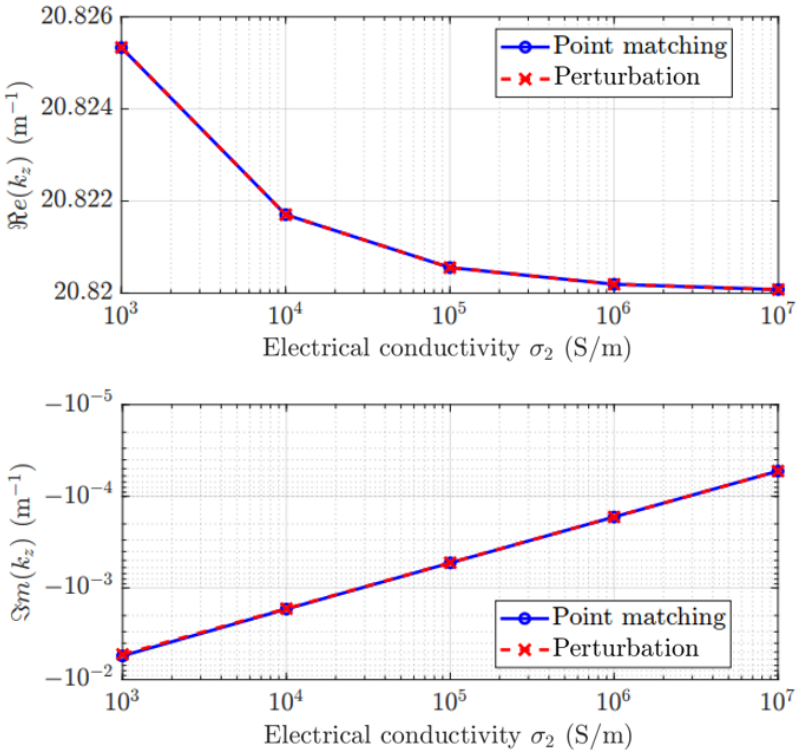

Figure 5.8: Longitudinal wavenumber of mode 2.

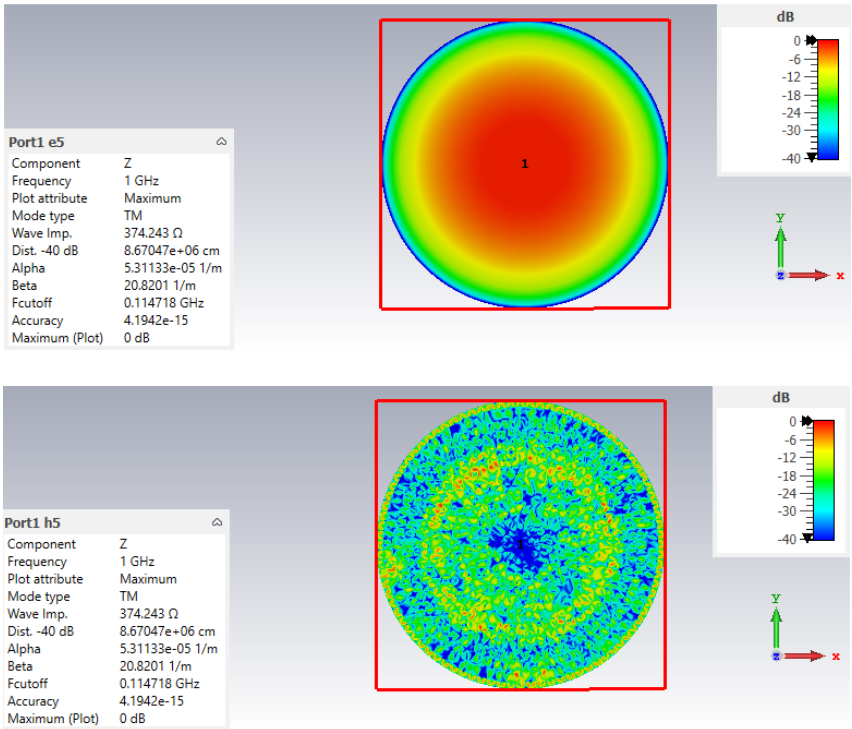

Figure 5.9: Normalized electric and magnetic fields E_z and H_z of mode 2 with $\sigma_2 = 10^7$ S/m via FEM.

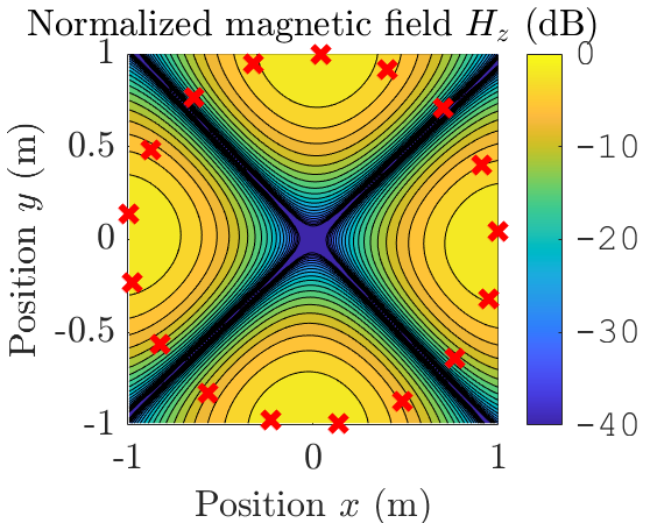

Figure 5.10: Normalized magnetic field H_z of mode 3 with $\sigma_2 = 10^7$ S/m.

at 1. The value of k_ρ was $3.0540 + j\ 2.7953 \times 10^{-4}$ m^{-1}, practically equal to the value of $x'_{np} = x'_{21}$ in Table 5-3 of [15].

Furthermore, from Fig. 5.11, it can be seen that $a_e < \eta\ a_h$, therefore, this mode is almost the TE^z_{21} mode.

Fig. 5.12 shows the longitudinal wavenumber of the third mode computed via the point matching solution and via the perturbation solution.

Fig. 5.13 shows the fields E_z and H_z produced via the finite element solution in the CST for mode 3. It can be seen that the value of k_z is in agreement with that found through the point matching algorithm ($k_z = 20.735 - j\ 4.1172 \times 10^{-5}$ m^{-1}).

5.1.1.4 Circular Waveguide with $\sigma_2 = 10^4$ S/m for the 1st Propagating Mode

For this example, we used an "imperfect" conductivity, meaning we chose a conductivity value lower than that of the previous examples. The normalized H_z field is shown in Fig. 5.14, and the modal amplitudes of the fundamental mode are illustrated in Fig. 5.15, where we observe a quasi-TE^z_{11} field.

The found value of the radial wavenumber was $k_\rho = 1.8331 + j\ 8.2938 \times 10^{-3}$ m^{-1}. As we decrease the value of the surface conductivity of the waveguide's cross-section, the value of k_ρ deviates slightly from the theoretical value compared to the value of k_ρ in Section 5.1.1.1 (the imaginary part of k_ρ increases with the inverse of σ_2).

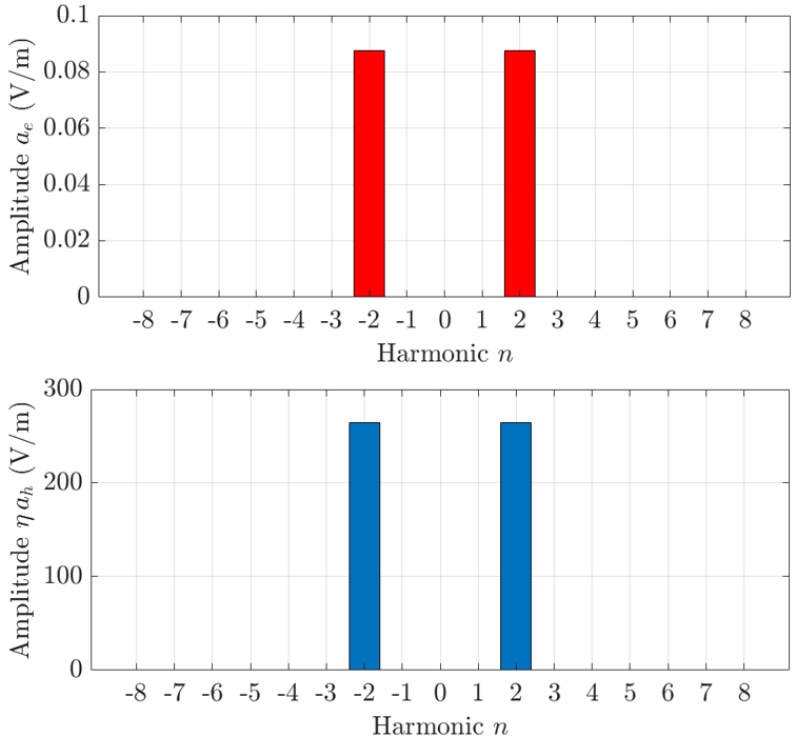

Figure 5.11: Modal amplitudes of mode 3 for the case $\sigma_2 = 10^7$ S/m.

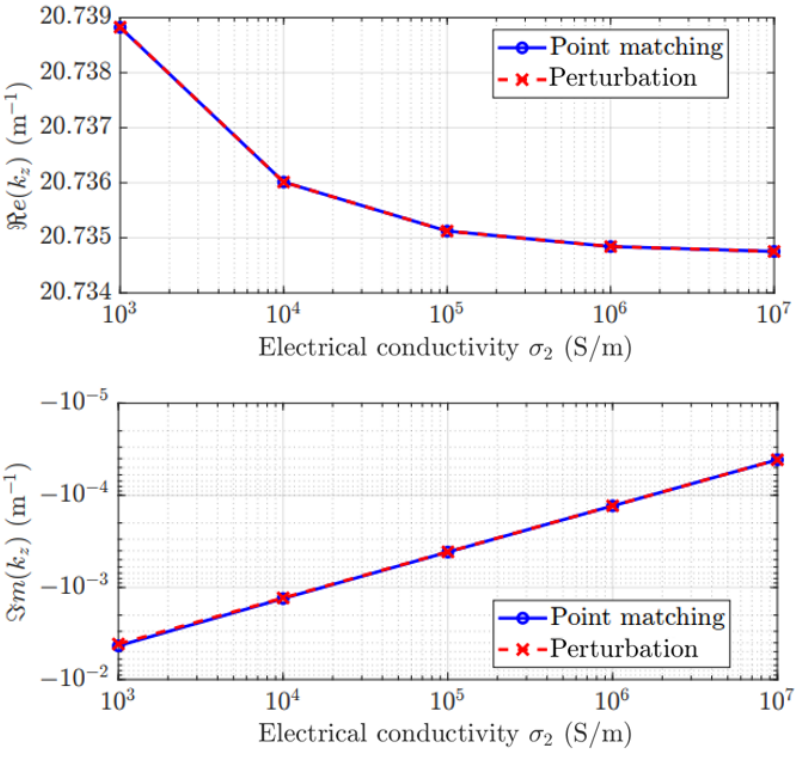

Figure 5.12: Longitudinal wavenumber of mode 3.

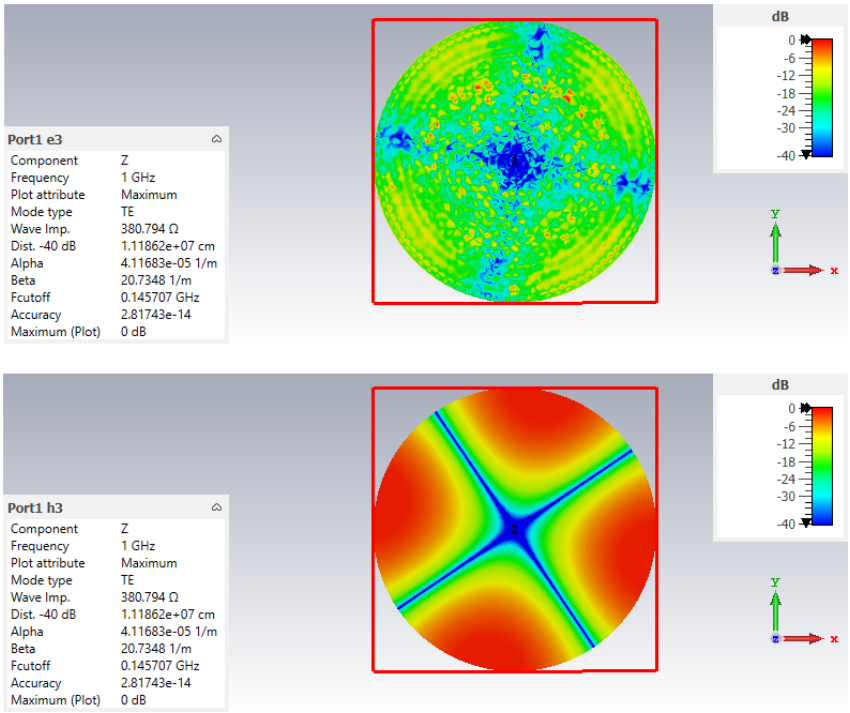

Figure 5.13: Normalized electric and magnetic fields E_z and H_z of mode 3 with $\sigma_2 = 10^7$ S/m via FEM.

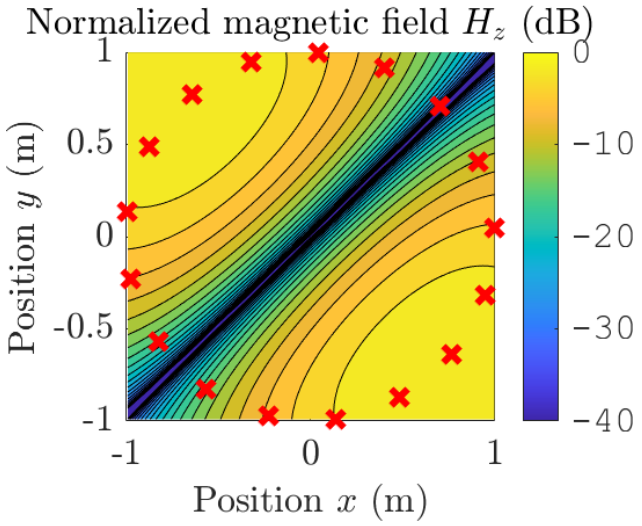

Figure 5.14: Normalized magnetic field H_z of mode 1 with $\sigma_2 = 10^4$ S/m.

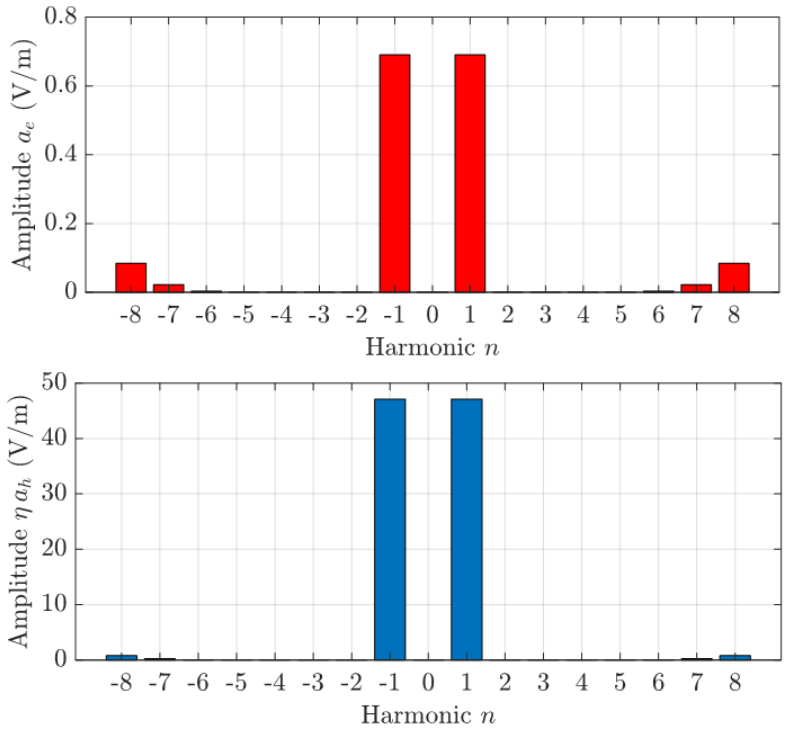

Figure 5.15: Modal amplitudes of mode 1 for the case $\sigma_2 = 10^4$ S/m.

5.1.1.5 Comparison of k_z value between PMM and FEM for the case $\sigma_2 = 10^7$ S/m

Table 5.1 shows the real and imaginary part of the longitudinal wavenumber k_z found using the point matching technique and the FEM of the CST software for each of the modes presented previously. The relative error regarding the real and imaginary part of k_z based on the comparison of the results obtained by the two methods are in Table 5.2. FEM solutions are used as reference.

Table 5.1: Real and imaginary part of the longitudinal wavenumber k_z of the first three modes in a circular waveguide obtained by PMM and FEM.

	Modo 1	Modo 2	Modo 3
$\Re e(k_z)_{PMM}$	20.877443	20.820078	20.734753
$\Im m(k_z)_{PMM}$	2.257676×10^{-5}	5.311193×10^{-5}	4.117159×10^{-5}
$\Re e(k_z)_{FEM}$	20.8774	20.8201	20.7348
$\Im m(k_z)_{FEM}$	2.25783×10^{-5}	5.31133×10^{-5}	4.11683×10^{-5}

5.1.1.6 Conclusion of Circular Waveguide Results

The analysis of the results obtained for the circular waveguide reveals important observations about the propagation modes and their characteristics. In all the studied modes, the maximum electric and magnetic fields behaved

Table 5.2: Relative error of the real and imaginary part of the longitudinal wavenumber k_z of the first three modes in a circular waveguide with respect to our method and the method used in CST.

	Modo 1	Modo 2	Modo 3
Relative Error - $\Re e(k_z)$ (%)	0.0002060	0.0001057	0.0002267
Relative Error - $\Im m(k_z)$ (%)	0.006821	0.002579	0.007992

consistently with theoretical expectations, confirming the validity of the method used here.

For the case of degenerate modes (different modes having the same cutoff frequency), we proceed as follows: after locating a "multiple" eigenvalue and the corresponding eigenvector, the characteristic equation is deflated to place a pole at the position of the found eigenvalue. Next, a new search for local minima is performed, and the eigenvalue is refined through a zero search. The new eigenvalue will be almost identical to the previous one. Using this last calculated eigenvalue, the singular value decomposition (SVD) technique is applied to find the associated eigenvector. In this way, it is observed that the last eigenvalue has associated fields that are orthogonal to those of the first one. The reason why the eigenvalues are not exactly equal is due to the selection of matching points, which are not perfectly symmetric along the contour.

The calculated values of k_ρ for each mode were close to the theoretical reference values, demonstrating the accuracy of the employed modeling. Additionally, the presence of hybrid components in the analyzed modes, especially in the TE^z_{11}, TM^z_{01} and TE^z_{21} modes, highlights the complexity of the electromagnetic interactions in these waveguides, indicating that the modes are not purely TE or TM but exhibit hybrid characteristics.

Finally, when comparing the results with reference solutions, such as those obtained by perturbation method and numerical solution via FEM in CST, a good agreement was observed, validating the use of the point matching method for the analysis of circular waveguides.

5.1.2 Truncated Elliptical Waveguide with Imperfect Walls

We consider an elliptical waveguide with radius $a = 1$ m and $b = 2$ m truncated with an imperfect conductor with $\sigma_2 = 10^5$ S/m, and $N = 8$ harmonics (with points equally spaced along the perimeter of the waveguide) in order to observe the electromagnetic propagation. The frequency used was 1 GHz.

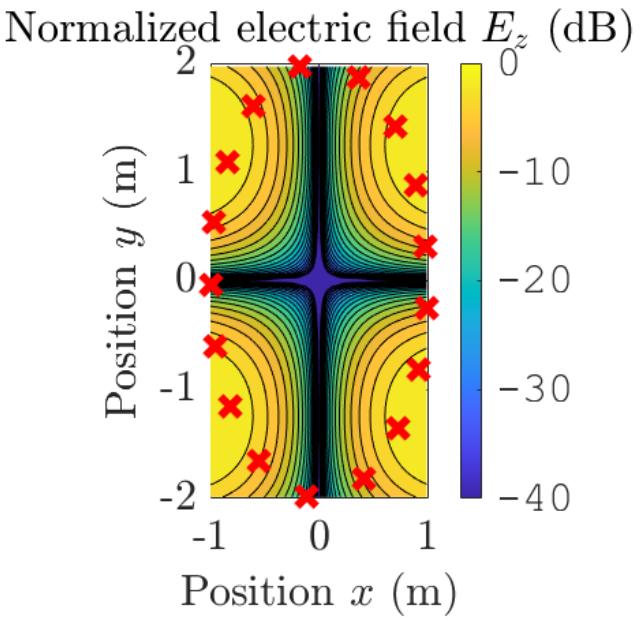

Figure 5.16: Normalized electric field E_z of mode 1 with $\sigma_2 = 10^5$ S/m.

5.1.2.1 Elliptical Waveguide with $\sigma_2 = 10^5$ S/m for the 1st Propagating Mode

For the first mode, the maximum field amplitudes found in the algorithm were: $E_{z_{\max}} = 0,20876$ and $H_{z_{\max}} = 0,092186$. Since there is a contribution from the electric field and $E_{z_{\max}} < \eta\, H_{z_{\max}}$, this is not a pure TE^z mode. Our solution via point matching provides mode 1 with $k_z = 20,889 - j\ 3,048 \times 10^{-4}$ m^{-1} for operation at 1 GHz. The associated longitudinal fields are shown in Figs. 5.16 and 5.17, where a quasi-TE^z field is observed. Additionally, from Fig. 5.18, we can see that $a_e < \eta\, a_h$.

In Fig. 5.19 we can observe the fields E_z and H_z produced via the finite element solution in the CST of mode 1. It is possible to verify that the value of k_z ($20,8889 - j\ 3,04841 \times 10^{-4}$ m^{-1}) is in agreement with that found through the point matching algorithm.

5.1.2.2 Elliptical Waveguide with $\sigma_2 = 10^5$ S/m for the 2nd Propagating Mode

For the second mode, the maximum field amplitudes found in the algorithm were: $E_{z_{\max}} = 0,59296$ and $H_{z_{\max}} = 0,34933$. Since there is a contribution from the electric field and $E_{z_{\max}} < \eta\, H_{z_{\max}}$, this is not a pure TE^z mode. Our solution via point matching provides mode 2 with $k_z = 20,884 - j\ 9,507 \times 10^{-5}$ m^{-1} for operation at 1 GHz. The associated longitudinal fields are shown in Figs. 5.20 and 5.21, where a quasi-TE^z field is observed. Additionally, from Fig. 5.22, we can see that $a_e < \eta\, a_h$.

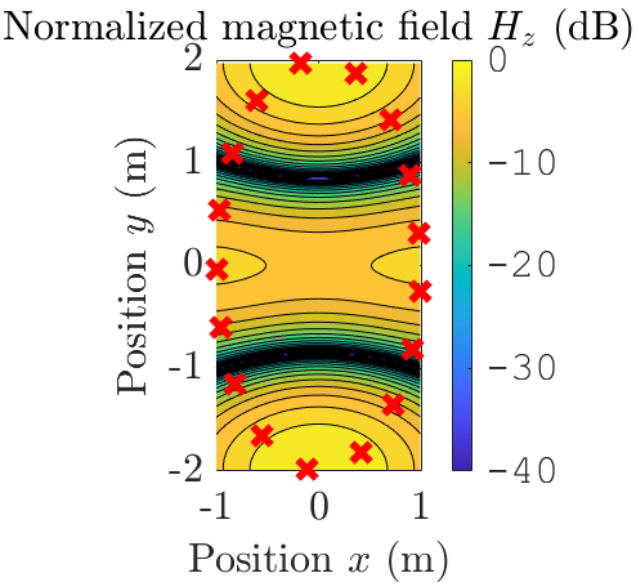

Figure 5.17: Normalized magnetic field H_z of mode 1 with $\sigma_2 = 10^5$ S/m.

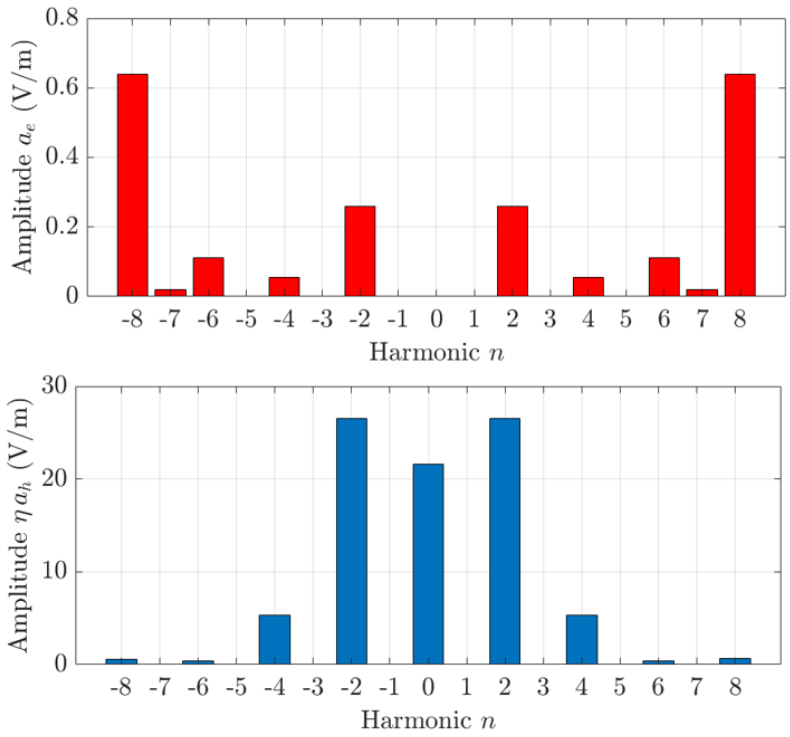

Figure 5.18: Modal amplitudes of mode 1 for the case $\sigma_2 = 10^5$ S/m.

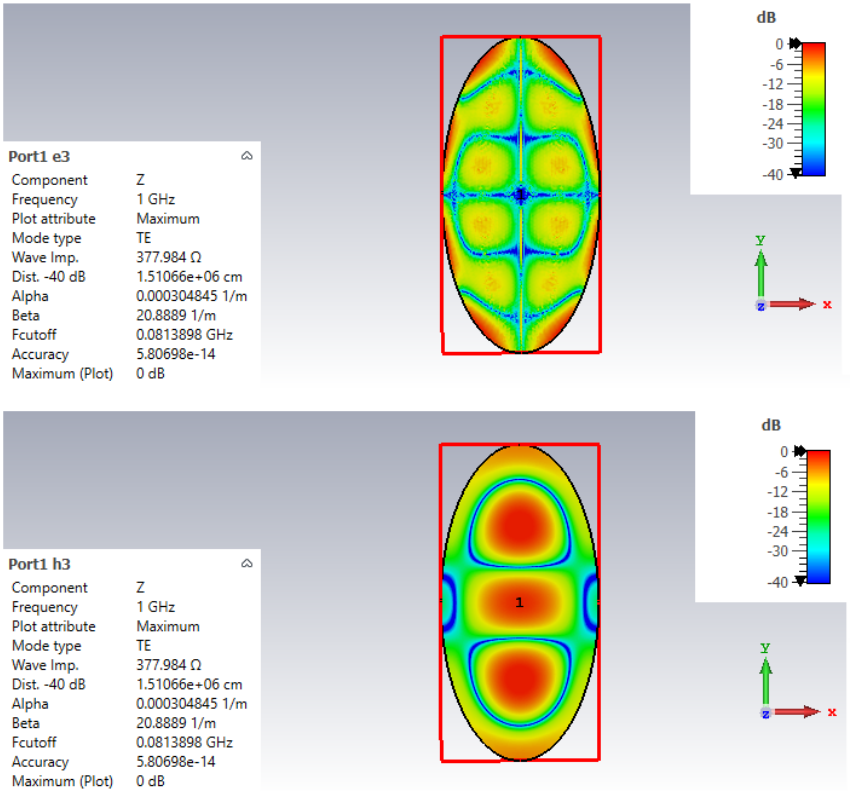

Figure 5.19: Normalized electric and magnetic fields E_z and H_z of mode 1 with $\sigma_2 = 10^5$ S/m via FEM.

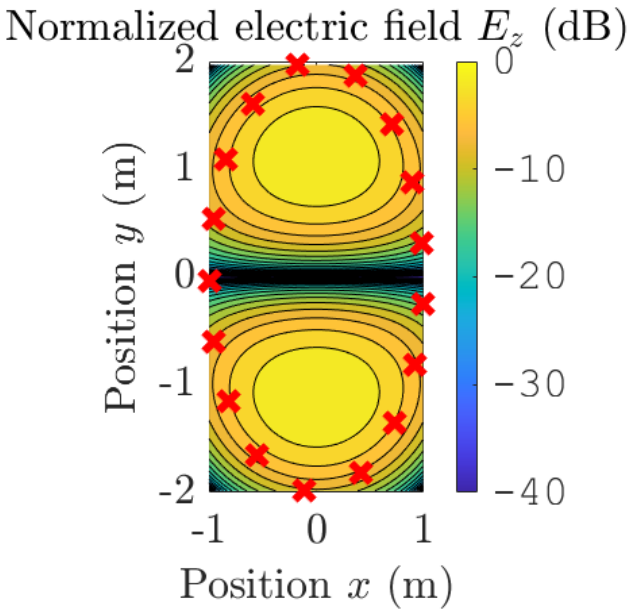

Figure 5.20: Normalized electric field E_z of mode 2 with $\sigma_2 = 10^5$ S/m.

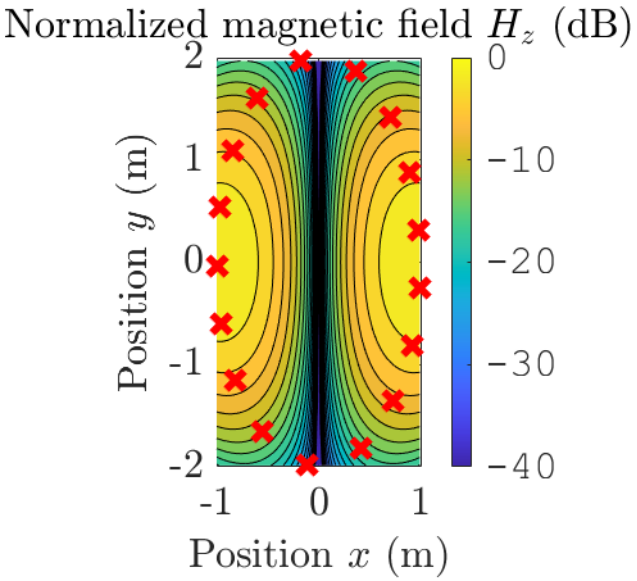

Figure 5.21: Normalized magnetic field H_z of mode 2 with $\sigma_2 = 10^5$ S/m.

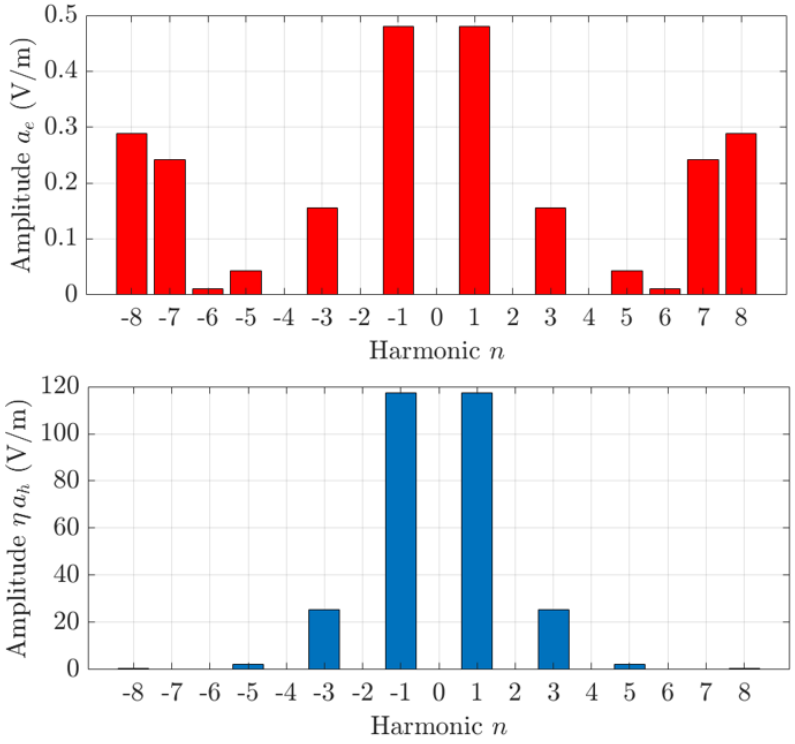

Figure 5.22: Modal amplitudes of mode 2 for the case $\sigma_2 = 10^5$ S/m.

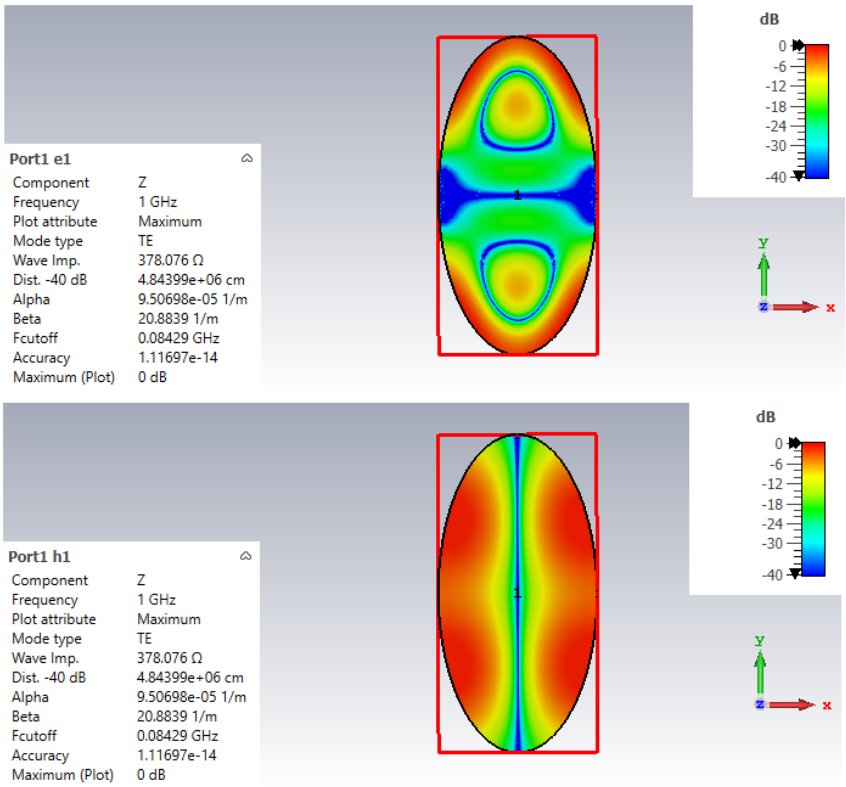

Figure 5.23: Normalized electric and magnetic fields E_z and H_z of mode 2 with $\sigma_2 = 10^5$ S/m via FEM.

In Fig. 5.23 we can observe the fields E_z and H_z produced via the finite element solution in the CST of mode 2. It is possible to verify that the value of k_z $(20,8839 - j\ 9,50677 \times 10^{-5}\ \mathrm{m}^{-1})$ is in agreement with that found through the point matching algorithm.

5.1.2.3 Elliptical Waveguide with $\sigma_2 = 10^5$ S/m for the 3rd Propagating Mode

For the third mode, the maximum field amplitudes found in the algorithm were: $E_{z_{\max}} = 0,84342$ and $H_{z_{\max}} = 1,1281 \times 10{-}5$. Since there is a contribution from the magnetic field and $E_{z_{\max}} > \eta\ H_{z_{\max}}$, this is not a pure TM^z mode. Our solution via point matching provides mode 3 with $k_z = 20,874 - j\ 4,829 \times 10^{-4}\ \mathrm{m}^{-1}$ for operation at 1 GHz. The associated longitudinal fields are shown in Figs. 5.24 and 5.25, where a quasi-TM^z field is observed. Additionally, from Fig. 5.26, we can see that $a_e < \eta\ a_h$.

In Fig. 5.27 we can observe the fields E_z and H_z produced via the finite element solution in the CST of mode 3. It is possible to verify that the value of k_z $(20,8737 - j\ 4,82879 \times 10^{-4}\ \mathrm{m}^{-1})$ is in agreement with that found through the point matching algorithm.

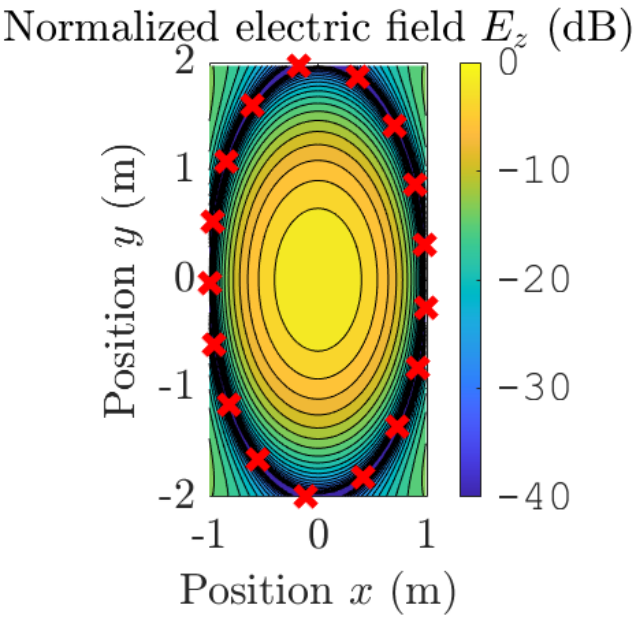

Figure 5.24: Normalized electric field E_z of mode 3 with $\sigma_2 = 10^5$ S/m.

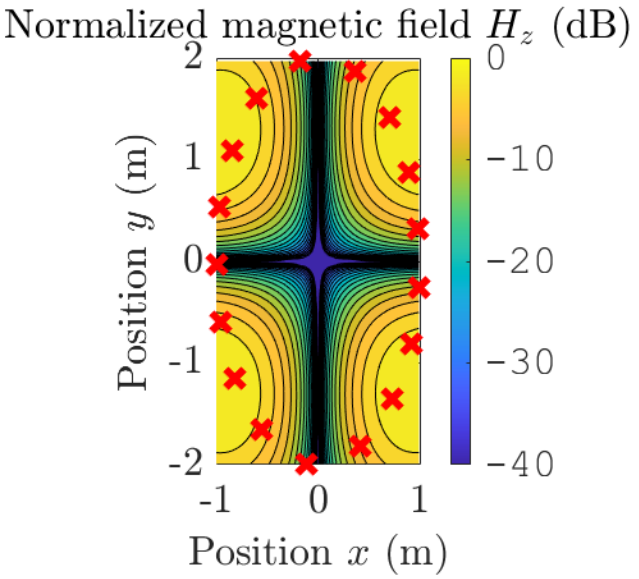

Figure 5.25: Normalized magnetic field H_z of mode 3 with $\sigma_2 = 10^5$ S/m.

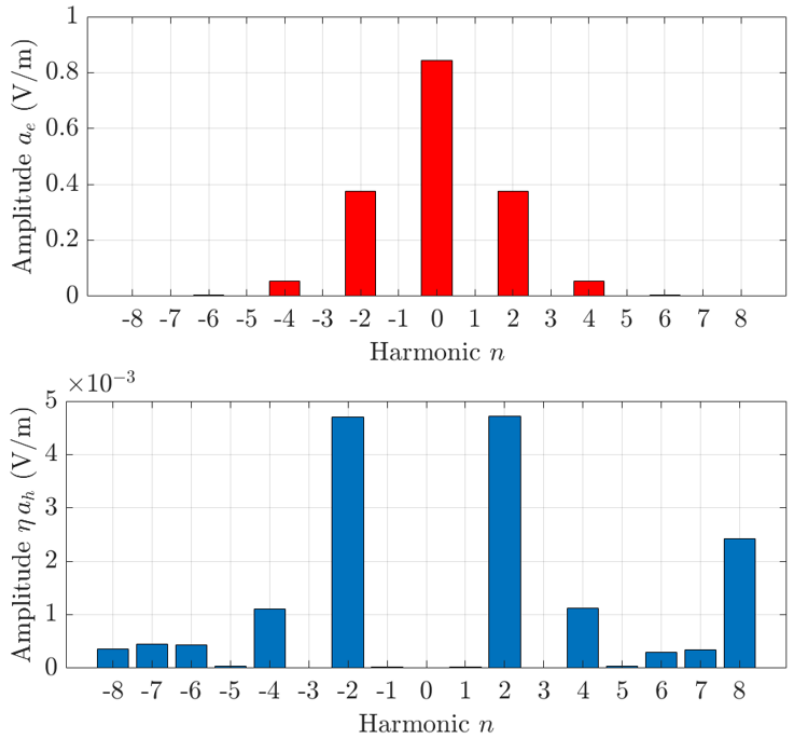

Figure 5.26: Modal amplitudes of mode 3 for the case $\sigma_2 = 10^5$ S/m.

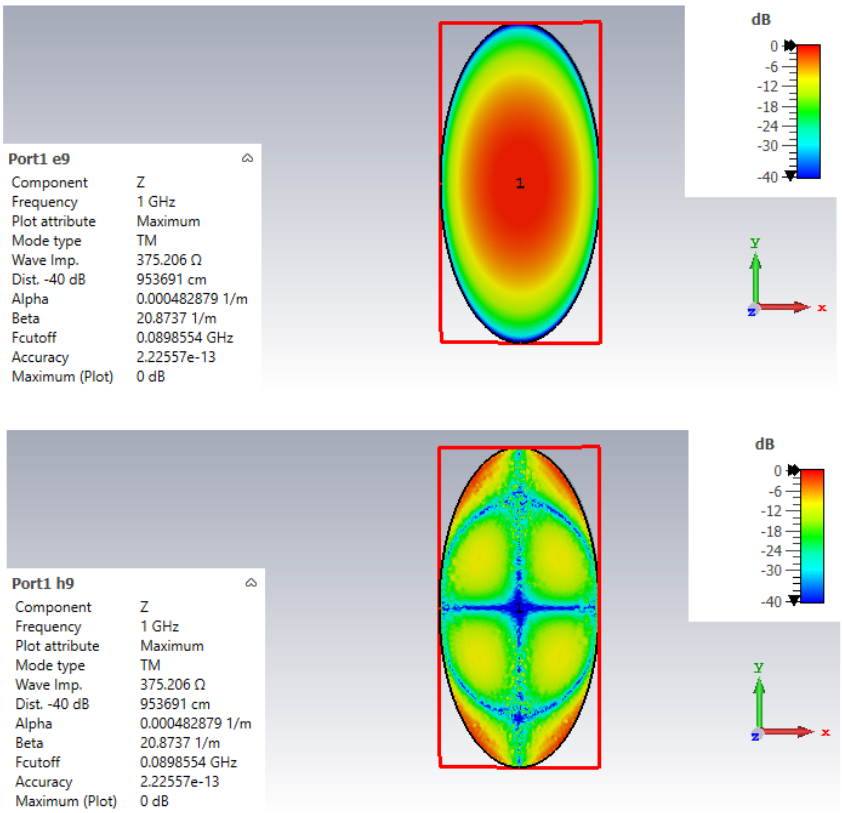

Figure 5.27: Normalized electric and magnetic fields E_z and H_z of mode 3 with $\sigma_2 = 10^5$ S/m via FEM.

5.1.2.4
Comparison of k_z value between PMM and FEM for the case $\sigma_2 = 10^5$ S/m

Table 5.3 shows the real and imaginary part of the longitudinal wavenumber k_z found using the point matching method and the FEM of the CST software for each of the previously presented modes of the elliptical waveguide case. The relative error regarding the real and imaginary part of k_z based on the comparison of the results obtained by the two techniques are in Table 5.4. FEM solutions are used as reference.

Table 5.3: Real and imaginary part of the longitudinal wavenumber k_z of the first three modes in a elliptical waveguide obtained by PMM and FEM.

	Modo 1	Modo 2	Modo 3
$\Re e(k_z)_{PMM}$	20.888917	20.883864	20.873666
$\Im m(k_z)_{PMM}$	3.048391×10^{-4}	9.506765×10^{-5}	4.828986×10^{-4}
$\Re e(k_z)_{FEM}$	20.8889	20.8839	20.8737
$\Im m(k_z)_{FEM}$	3.04845×10^{-4}	9.50698×10^{-5}	4.82879×10^{-4}

Table 5.4: Relative error of the real and imaginary part of the longitudinal wavenumber k_z of the first three modes in a elliptical waveguide with respect to our method and the method used in CST.

	Modo 1	Modo 2	Modo 3
Relative Error - $\Re e(k_z)$ (%)	0.00008138	0.0001724	0.0001629
Relative Error - $\Im m(k_z)$ (%)	0.001935	0.002261	0.004059

5.1.2.5
Conclusion of Elliptical Waveguide Results

The application of the point matching method (PMM) to the examples of elliptical waveguides demonstrated consistent results in obtaining the quasi-TE^z and quasi-TM^z modes, as evidenced by the electric and magnetic field distributions. The comparison with the finite element method (FEM) from the CST software revealed good agreement in both the longitudinal fields E_z and H_z and the values of the longitudinal wavenumber k_z, with minor deviations due to differences in the numerical approaches of each technique.

An important point to mention is that FEM is a numerical solution but not a physical one. As a result, some of the fields generated in CST do not exhibit symmetry, requiring the use of a symmetric plane for the simulation. Additionally, some modes exhibit fields that appear spurious (irregular or non-physical field patterns). This does not occur with the fields generated by PMM, which represent more physical and symmetric fields. Therefore, PMM has proven to be an efficient solution for modal analysis.

6
Conclusions and Future Works

Isotropic or anisotropic guided cylindrical structures, such as coaxial cables and waveguides, are widely used in microwave and millimeter-wave systems, with their electromagnetic analysis obtained through numerical or analytical models. An example is the point matching method, a semi-analytical approach where the solution is obtained by imposing boundary conditions at discrete points along the domain boundaries, using analytical expansions. Another example is the finite element method, a fully numerical technique in which the domain is divided into small finite elements, and shape functions are used to interpolate the values of the variables within each element.

In this work, we present a brief theoretical review of cylindrical wave functions in Chapter 2 to address physical and mathematical problems involving cylindrical symmetry, such as the propagation of electromagnetic waves in cylindrical structures.

Chapter 3 presents a theoretical analysis of waveguides with arbitrarily shaped cross-sections and straight longitudinal axes truncated by an impedance boundary condition. Through the impedance boundary condition equation on a high-conductivity surface, we derive expressions for the modal fields within the waveguide.

In Chapter 4, we introduce a mathematical model for analyzing hollow waveguides with arbitrary cross-sections, employing an approach based on the expansion of cylindrical harmonics and the point-matching method.

The numerical results for different cross-section geometries and conductivities are presented in Chapter 5. These results validate the proposed model, which proves capable of handling different impedance boundary conditions, offering a robust tool for waveguide analysis in various configurations. Its advantage over brute-force approaches lies in its lower computational resource requirements.

Comparing the results of the technique explored here with the perturbation method and the finite element method (FEM) used in the CST software for the frequency of 1 GHz, we observed good agreement with small deviations due to the different numerical methods employed. It is worth highlighting that in the CST there is a problem of convergence of the FEM (non-physical solution),

with the emergence of spurious modes and thus compromising the accuracy of the simulation in the CST.

These techniques also work for frequencies of 30 GHz and above. The higher-order terms with $k_2\ \rho$ become smaller as the frequency increases and as the radius of curvature ρ of the contour bounding the waveguide increases. Another point, further confirming that the solution is suitable for millimeter waves, is that the expansion of the fields in Maxwell's equations uses Bessel-Fourier harmonics, which we know solve the truncation problem by PEC ($Z_2 = 0$) exactly. Since the impedance of medium 2 is such that $Z_2 = \sqrt{\mu_0/\epsilon_2}$, with $\epsilon_2 = \epsilon_0\epsilon_{r_2} - j\ \sigma_2/\omega$, if the frequency increases, Z_2 will be small.

Future research may explore applying this method to other complex geometries. Additionally, we recommend studying the first-order Rytov boundary condition, which is essential for analyzing modal fields in waveguides with anisotropic properties. Finally, another aspect worth investigating is the expansion of sources within waveguides truncated by higher-order impedance boundary conditions to analyze wireless communication along realistic tunnels. Based on Lorentz's reciprocity theorem, it is possible to introduce an expansion of the electromagnetic source in terms of cylindrical harmonics.

Bibliography

[1] J. Whinnery and H. Jamieson, "Equivalent circuits for discontinuities in transmission lines," *Proceedings of the IRE*, vol. 32, no. 2, pp. 98–114, 1944.

[2] N. Marcuvitz, "Waveguide handbook (ieee electromagnetic waves series)," *The Institution of Engineering and Technology*, 1986.

[3] J. R. Gonçalves, "Semi-analytical methods for the electromagnetic propagation analysis of inhomogeneous anisotropic waveguides of arbitrary cross-section by using cylindrical harmonics," Ph.D. dissertation, PUC-Rio, 2022.

[4] W. T. Shaw and A. J. Dougan, "Curvature corrected impedance boundary conditions in an arbitrary basis," *IEEE transactions on antennas and propagation*, vol. 53, no. 5, pp. 1699–1705, 2005.

[5] A. Ghuniem, "Modes of electromagnetic wave propagation in circular concrete tunnels," *Journal of Electromagnetic Waves and Applications*, vol. 19, no. 1, pp. 95–106, 2005.

[6] G. S. Rosa, "A robust method for solving the modal fields in radially unbounded cylindrical waveguides with two layers under extreme conductive conditions," *IEEE Transactions on Antennas and Propagation*, vol. 70, no. 7, pp. 5841–5848, 2022.

[7] C. L. Holloway, D. A. Hill, R. A. Dalke, and G. A. Hufford, "Radio wave propagation characteristics in lossy circular waveguides such as tunnels, mine shafts, and boreholes," *IEEE transactions on antennas and propagation*, vol. 48, no. 9, pp. 1354–1366, 2000.

[8] X. Zhang and C. D. Sarris, "Statistical modeling of electromagnetic wave propagation in tunnels with rough walls using the vector parabolic equation method," *IEEE Transactions on Antennas and Propagation*, vol. 67, no. 4, pp. 2645–2654, 2019.

[9] L. Tsang, J. Kong, and K.-H. Ding, "Scattering of electromagnetic waves: Theories and applications. john wisley & sons," 2000.

[10] S. Caorsi, M. Pastorino, and M. Raffetto, "Electromagnetic scattering by a multilayer elliptic cylinder under transverse-magnetic illumination: Series

solution in terms of mathieu functions," *IEEE Transactions on Antennas and Propagation*, vol. 45, no. 6, pp. 926–935, 1997.

[11] G. S. DA ROSA, "Electromagnetics wave propagation in coaxial guides with non-homogeneous load excited by the tem mode," 2013.

[12] W. C. Gibson, *The method of moments in electromagnetics*. Chapman and Hall/CRC, 2021.

[13] D. B. Davidson, *Computational electromagnetics for RF and microwave engineering*. Cambridge University Press, 2010.

[14] R. L. Silvester, Peter Peet; Ferrari, *Finite elements for electrical engineers*. Cambridge University Press, 1996.

[15] R. F. Harrington, *Time-Harmonic Electromagnetic Fields*. New York, NY, USA: McGraw-Hill, 1961.

[16] R. Bates and F. Ng, "Point matching computation of transverse resonances," *International Journal for Numerical Methods in Engineering*, vol. 6, no. 2, pp. 155–168, 1973.

[17] S. V. Yuferev and N. Ida, *Surface impedance boundary conditions: a comprehensive approach*. CRC press, 2018.

[18] C. A. Balanis, *Advanced engineering electromagnetics*. John Wiley & Sons, 2012.

[19] T. B. Senior and J. L. Volakis, *Approximate boundary conditions in electromagnetics*. Iet, 1995, no. 41.

[20] T. B. Senior, J. L. Volakis, and S. R. Legault, "Higher order impedance and absorbing boundary conditions," *IEEE Transactions on Antennas and Propagation*, vol. 45, no. 1, pp. 107–114, 1997.

[21] T. Senior, "Approximate boundary conditions," *IEEE Transactions on Antennas and Propagation*, vol. 29, no. 5, pp. 826–829, 1981.

[22] N. Audeh and J. Fuller, "The point-matching solution of uniform nonsymmetric waveguides." 1969.

[23] H. Yee and N. Audeh, "Uniform waveguides with arbitrary cross-section considered by the point-matching method," *IEEE Transactions on Microwave Theory and Techniques*, vol. 13, no. 6, pp. 847–851, 1965.

[24] MATLAB, *version 9.13.0.2080170 (R2022b) Update 1*. Natick, Massachusetts: The MathWorks Inc., 2022.

[25] CST AG, CST Studio Suite 2019, Darmstadt, Germany, 2019.

A
First-Order Rytov Boundary Condition

In this case, we will consider the same waveguide represented in Fig. 3.1 and define the unit normal vector to the surface only in the radial direction, i.e., $\hat{n} = \hat{\rho}$. For a cylindrical surface $\rho =$ constant, the impedance of the surrounding medium is anisotropic, that is, it is the local tensor with components in the azimuthal and axial directions. The first-order Rytov impedance boundary condition on the contour C is given by [19, 20]

$$\hat{n} \times \bar{E} = \bar{\bar{\eta}} \cdot \hat{n} \times \left(\hat{n} \times \bar{H}\right). \tag{A-1}$$

Based on the equations [19]

$$E_\alpha = -Z\ H_\beta\ \left\{1 - \frac{1}{2\ j\ k_0\ N\ h_\gamma}\frac{\partial}{\partial\gamma}\left(ln\left(\frac{h_\alpha}{h_\beta}Z\right)\right)\right\} \tag{A-2}$$

$$E_\beta = Z\ H_\alpha\ \left\{1 - \frac{1}{2\ j\ k_0\ N\ h_\gamma}\frac{\partial}{\partial\gamma}\left(ln\left(\frac{h_\beta}{h_\alpha}Z\right)\right)\right\}, \tag{A-3}$$

it is sufficient to convert the constant impedance Z of contour C into its anisotropic form. Thus, the fields will take the following form [19, 21]:

$$E_\phi = -Z\ H_z\ \left\{1 - \frac{1}{2\ j\ k_0\ N\ h_\rho}\frac{\partial}{\partial\rho}\left(ln\left(\frac{h_\phi}{h_z}Z\right)\right)\right\} \tag{A-4}$$

$$E_z = Z\ H_\phi\ \left\{1 - \frac{1}{2\ j\ k_0\ N\ h_\rho}\frac{\partial}{\partial\rho}\left(ln\left(\frac{h_z}{h_\phi}Z\right)\right)\right\} \tag{A-5}$$

The effective surface impedance implicit in (A-4) and (A-5) is a tensor with components

$$\eta_{\phi\phi} = Z\ \left\{1 - \frac{1}{2\ j\ k_0\ N\ h_\rho}\frac{\partial}{\partial\rho}\left(ln\left(\frac{h_z}{h_\phi}Z\right)\right)\right\}, \tag{A-6}$$

$$\eta_{zz} = Z\ \left\{1 - \frac{1}{2\ j\ k_0\ N\ h_\rho}\frac{\partial}{\partial\rho}\left(ln\left(\frac{h_\phi}{h_z}Z\right)\right)\right\}. \tag{A-7}$$

Applying the metrics corresponding to the cylindrical coordinate system ($h_\phi = \rho, h_\rho = h_z = 1$) and assuming that $N = \sqrt{\epsilon\mu/\epsilon_0\mu_0} = k/k_0$, ($k = k_2$), which is the complex refractive index, we have that

$$\eta_{\phi\phi} = Z \left\{1 - \frac{1}{2\ j\ k_2} \frac{\partial}{\partial \rho} \left(ln \left(\frac{1}{\rho} Z \right) \right) \right\}, \tag{A-8}$$

$$= Z \left\{1 + \frac{1}{2\ j\ k_2\ \rho} \right\}, \tag{A-9}$$

$$\eta_{zz} = Z \left\{1 - \frac{1}{2\ j\ k_2} \frac{\partial}{\partial \rho} \left(ln \left(\rho Z \right) \right) \right\}, \tag{A-10}$$

$$= Z \left\{1 - \frac{1}{2\ j\ k_2\ \rho} \right\}, \tag{A-11}$$

$$E_\phi = -\eta_{zz}\ H_z = -Z \left\{1 - \frac{1}{2\ j\ k_2\ \rho} \right\}\ H_z, \tag{A-12}$$

$$E_z = \eta_{\phi\phi}\ H_\phi = Z \left\{1 + \frac{1}{2\ j\ k_2\ \rho} \right\}. \tag{A-13}$$